Electronic Supplementary Information for

Aryl Imidazoisoindoles for Mesomeric 6π and Intrinsic 10π Pericyclic Photochromism and Non-linear Acid Responsiveness

Taichi Muto[1,2], Chigusa Goto[1,3], Shohei Katao[3], Tsuyoshi Kawai[1, 2, 4]

1: Laboratory for Photonic and Reactive Molecular Science, Graduate School of Science and Technology, Nara Institute of Science and Technology, NAIST, 1 8916-5 Takayama, Ikoma, Nara 630-0192, Japan

2: International Collaborative Laboratory for Interfaces, Molecules and Materials, NAIST - Université de Toulouse, 118 route de Narbonne, 31062 Toulouse Cedex 9, France

3: Center for Materials Research Platform, Nara Institute of Science and Technology, NAIST, 1 8916-5 Takayama, Ikoma, Nara 630-0192, Japan

4: Medilux Research Center, Nara Institute of Science and Technology, NAIST, 1 8916-5 Takayama, Ikoma, Nara 630-0192, Japan

*Corresponding author: E-mail: tkawai@ms.naist.jp

1. General

General chemicals were purchased from Tokyo Chemical Industry (TCI), Wako Pure Chemicals, or Sigma Aldrich Chemicals Co., and used without further purification. Silica gel column chromatography was performed using silica gel 60N (spherical neutral, particle size 63–210 μm). Recycling preparative GPC separation was performed with a LaboACE LC-5060 (Japan Analytical Industry Co., Ltd). NMR spectra were recorded on a JEOL JNM-ECA600 (600 MHz) and JEOL JNM-ECZ500R (500 MHz). High-resolution mass spectra (HRMS) were measured on a JMS-S3000 (MALDI-Spiral-TOFMS) mass spectrometer.

Single-crystal X-ray crystallographic analysis was performed using a Rigaku XtaLAB Synergy (1.2 kW) diffractometer with photon Jet-R rotating anode X-ray source CuKα radiation and Hypix-6000HE detector. A single crystal for diffraction measurement was mounted with epoxy resin on a glass fiber, the temperature of which was controlled using a nitrogen gas-flow. The collected X-ray diffraction data were processed using CrysAlisPro. The obtained data were solved with the SHELXT structure solution program and refined with the SHELXL refinement package using Olex2 ver1.5. Hydrogen atoms were refined using the riding model.

UV-vis absorption spectra were recorded using a JASCO V-550 or V-760 spectrometer. The temperature was controlled by a JASCO ETC 505T temperature controller. The quantum yields of photocyclization and photocycloreversion were measured using a Shimadzu QYM-01. Emission and excitation spectra were measured using a JASCO FP-8500 spectrometer. Emission quantum yield was measured using a Hamamatsu Photonics C9920-02 instrument with an integrating sphere.

The optimized structures of the ground state and molecular orbitals were calculated by the density functional theory (DFT) and time-dependent density functional theory (TD-DFT) method at the M062x/6-311+G(d,p) level of theory. NICS(0)zz values were calculated by the gauge-independent atomic orbital (GIAO method) at the M062x/6-311+G(d,p) level of theory. The Banquo atoms were placed on the centroid of the rings, and the NMR shift was calculated.

The transition-state search for **2o**/**2c** and **2oH**/**2cH** was performed using the Opt=TS keyword with the Berny algorithm. To follow the unrestricted Kohn–Sham solution, a broken-symmetry guess was generated and applied using the keyword Guess=(Mix,Always) in **2o**/**2c**. The optimized structures of the open- and closed-ring isomers, as well as the transition state, were characterized by frequency calculations at the same level of theory (the number of imaginary frequencies was 1 for the transition state and 0 for the local minima). Intrinsic reaction coordinate (IRC) calculations for **2oH**/**2cH** were carried out to confirm that the transition state connects the open- and closed-ring isomers.

The PECs along the corresponding reaction coordinate on the S0 state were recorded by a relaxed scan approach, and geometry optimization was performed at each step with the scanned variable maintained constant. The excited state scans were done for the same steps as the ground state scan. For the excited state scans, we performed single-point energy calculations for the corresponding optimized geometries of the ground state.

All calculations were carried out using the Gaussian16 package.

2. Synthesis

The synthesis route to **1o**/**1e** and **2o**/**2e** are illustrated in scheme S1. Detailed synthetic procedures of these molecules are described below. 5H-imidazo[5,1-a] isoindole (**3**) was prepared according to the procedures reported by T. Muto *et al*. and the NMR and MS data were identical with the literature.[S1]

Scheme S1

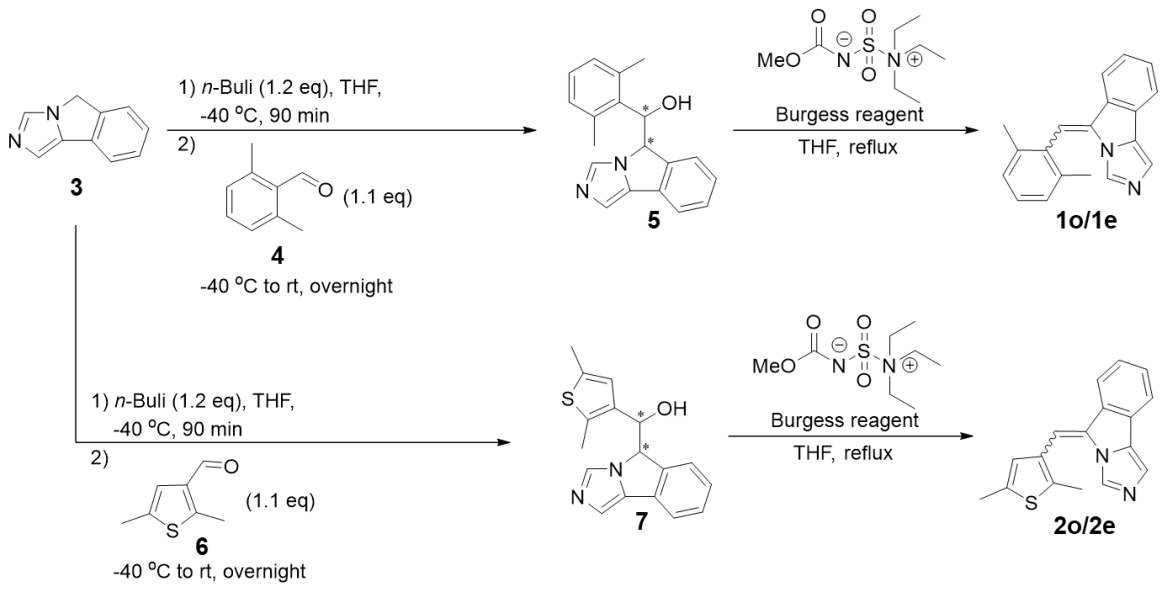

Compound 5

To a solution of **3** (700 mg, 4.48 mmol, 1.0 eq.) in anhydrous THF (20 mL) at −40° C was added *n*-BuLi(3.8 mL, 6.1 mmol, 1.4 eq., 1.6 M solution hexanes) under Ar. After stirring for 90 min at −40 °C, a solution of compound **4** (740 mg, 5.52 mmol, 1.2 eq.) in THF (3 mL) was added and the reaction was allowed to warm to RT overnight and was quenched by adding sat. NH_4Cl aq. The reaction mixture was diluted with water, extracted with CH_2Cl_2 (3 × 100 mL). The combined organic extract was dried over Na_2SO_4 and concentrated under reduced pressure. The crude compound (1.12 g) was used in the next reaction without further purification. HRMS (MALDI): *m/z* calcd for $C_{19}H_{19}N_2O$ +: 291.1492 [M+H]+;found: 291.1495.

Compound 1o and 1e

Compound **5** (crude, 1.1 g, 3.8 mmol, 1.0 eq.) was dissolved in anhydrous THF (120 mL) and mixed with methoxy carbonyl sulfamoyl-triethylammonium hydroxide (Burgess reagent; 1.5 g, 6.3 mmol, 1.7 eq.). After stirring for 4 h at reflux under Ar, the reaction mixture was washed with sat. aqueous $NaHCO_3$ and extracted with CH_2Cl_2 (3 × 40 mL). The combined organic layers were dried over Na_2SO_4 and concentrated under reduced pressure. The crude was purified by silica-gel column chromatography eluted with MeOH/DCM (1:20) to afford compound **1o** (55.2 mg, 0.20 mmol, 5% yield in two steps) and **1e** (351 mg, 1.29 mmol, 34% yield in two steps).

1o: ^{1}H-NMR (500 MHz, CD_2Cl_2, ppm): δ = 7.79 (d, *J* = 6.0 Hz, 1H; H_f), 7.55 (d, *J* = 6.7 Hz, 1H; H_c), 7.43 (td, *J* =7.6 Hz, 1.0 Hz, 1H; H_d), 7.34 (td, *J* =7.6, 1.1 Hz, 1H; H_e), 7.26-7.24 (m, 1H; H_j), 7.20-7.18 (m, 2H; H_i and H_k), 7.03 (s, 1H; H_b), 6.96 (s, 1H; H_g), 6.66 (s, 1H; H_a), 2.24 (s, 6H; H_h and H_l). Quantitative ^{13}C-NMR (151 MHz, CD_2Cl_2, ppm): δ = 136.8-136.9 (3C), 136.5-136.6 (1C), 133.9-134.0 (1C), 133.5-133.6 (1C),

131.8-131.9 (1C), 129.9-130.1 (2C), 128.9-129.0 (1C), 128.6-128.7 (2C), 127.1-127.2 (1C), 122.0-122.1 (1C), 120.5-120.6 (1C), 119.3-119.3 (1C), 110.5-110.6 (1C), 20.2-20.3 (2C). HRMS (MALDI): *m/z* calcd for $[C_{19}H_{17}N_2]$ +: 273.1386 [M+H]+; found: 273.1384. The molecular structure in the crystal state was determined by single-crystal diffraction analysis. Orange crystal suitable for SC-XRD were obtained at ambient temperature by liquid-phase slowly diffusion of hexane into a concentrated solution of the compound in dichloromethane.

1e: ^{1}H-NMR (600 MHz, CD_2Cl_2, ppm): δ = 8.04 (s, 1H; H_a), 7.49 (d, J = 7.6 Hz, 1H; H_c), 7.29 (t, J = 7.6 Hz, 1H; H_d), 7.25 (t, J = 7.6 Hz, 1H; H_i), 7.18-7.16 (m, 2H; H_j and H_j), 7.09 (s, 1H; H_b), 7.07 (s, 1H; H_l), 6.95 (t, J = 8.2 Hz, 1H; H_e). 6.56 (d, J = 8.2 Hz, 1H; H_f), 2.25 (s, 6H; H_g and H_k). Quantitative ^{13}C-NMR (151 MHz, CD_2Cl_2, ppm): δ = 137.4 (s, 2C), 136.1 (s, 1C), 135.8 (s, 1C), 133.7 (s, 1C), 132.9 (s, 1C), 131.1 (s, 1C), 130.3 (s, 1C), 129.7 (s, 1C), 128.6 (s, 1C), 128.3 (s, 2C), 127.4 (s, 1C), 124.7 (s, 1C), 120.4 (s, 1C), 119.7 (s, 1C), 112.7 (s, 1C), 20.7 (s, 2C). HRMS (MALDI): *m/z* calcd for $[C_{19}H_{17}N_2]$ +: 273.1386 [M]+; found: 273.1387.

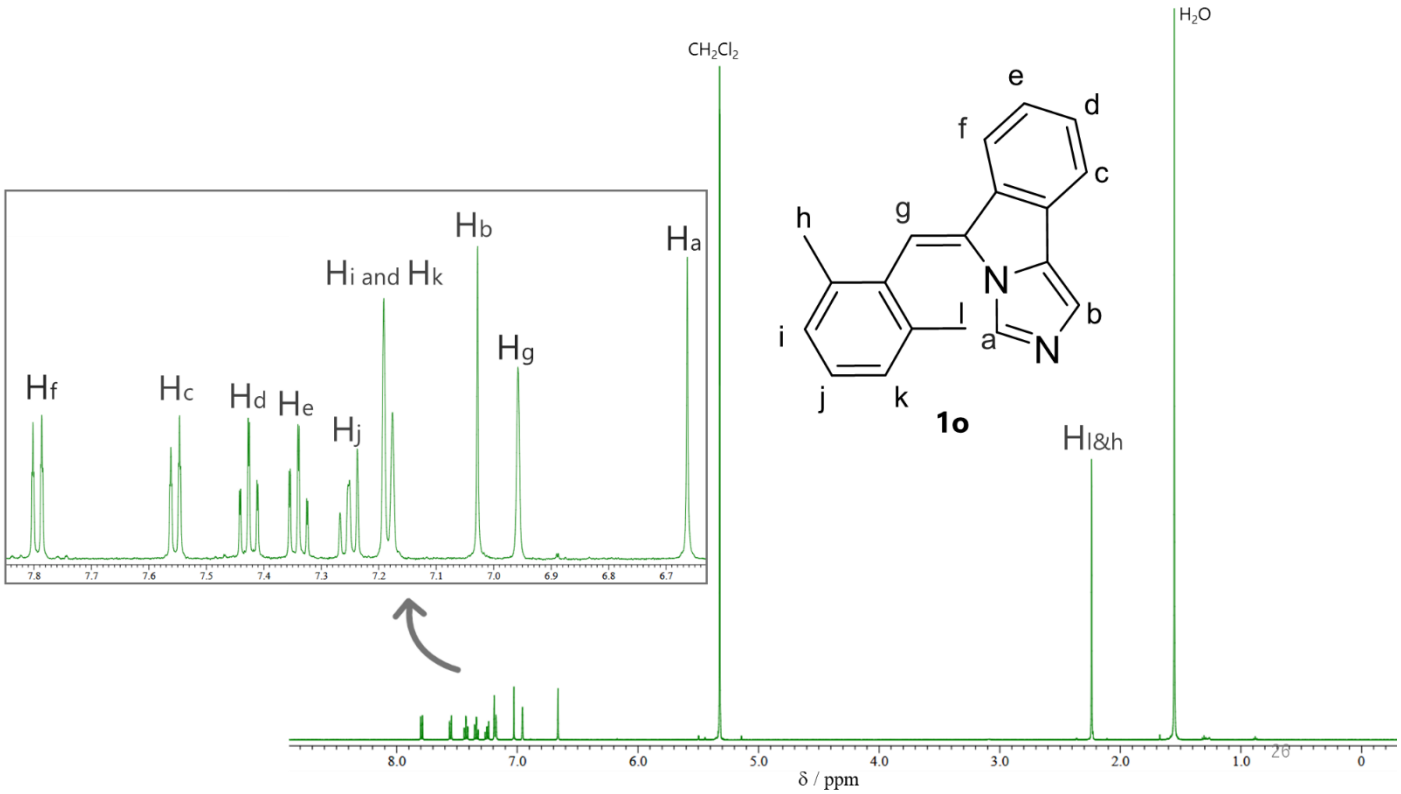

Figure S1. ^{1}H-NMR spectrum of compound **1o**

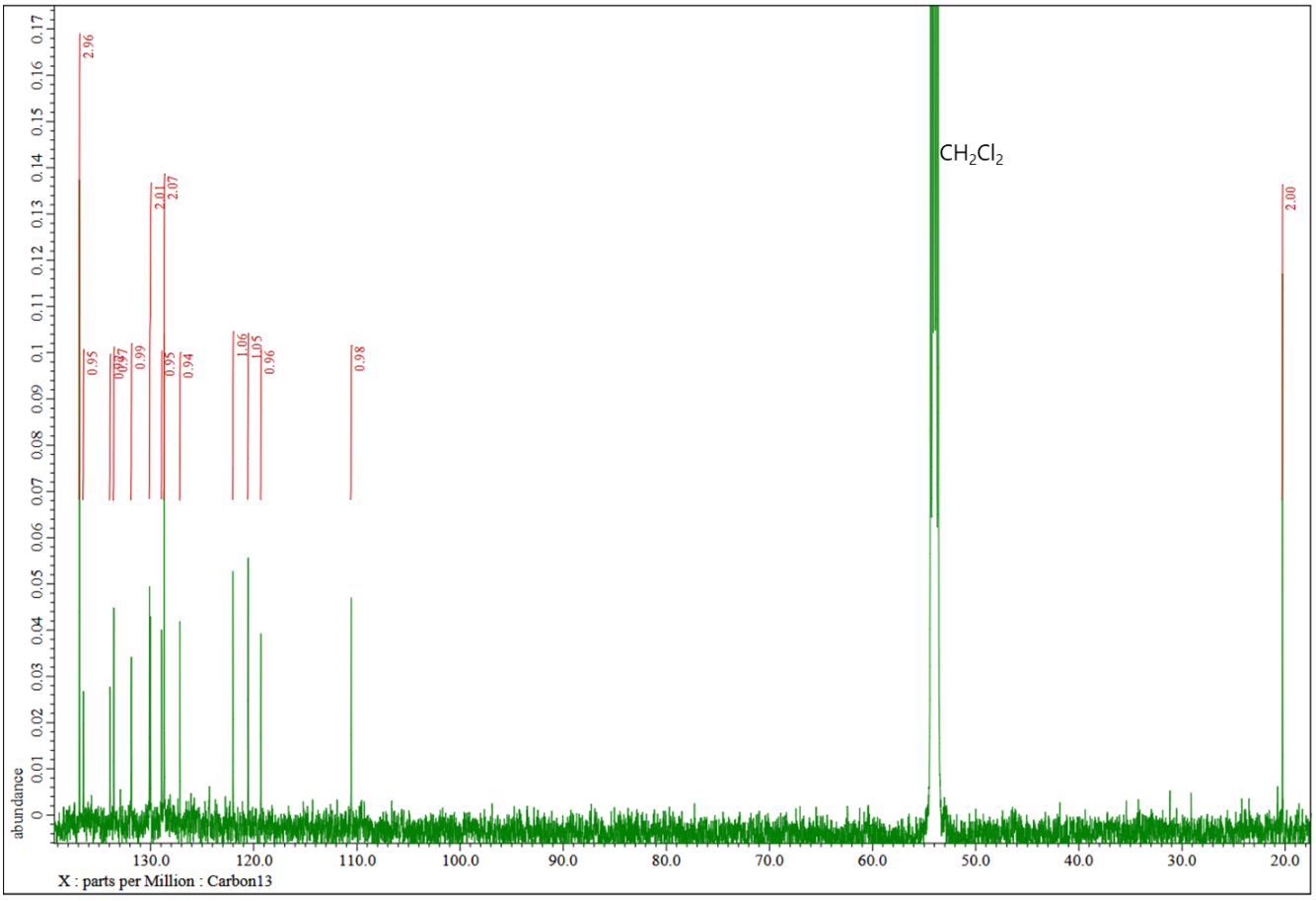

Figure S2. ^{13}C-NMR spectrum of compound **1o**

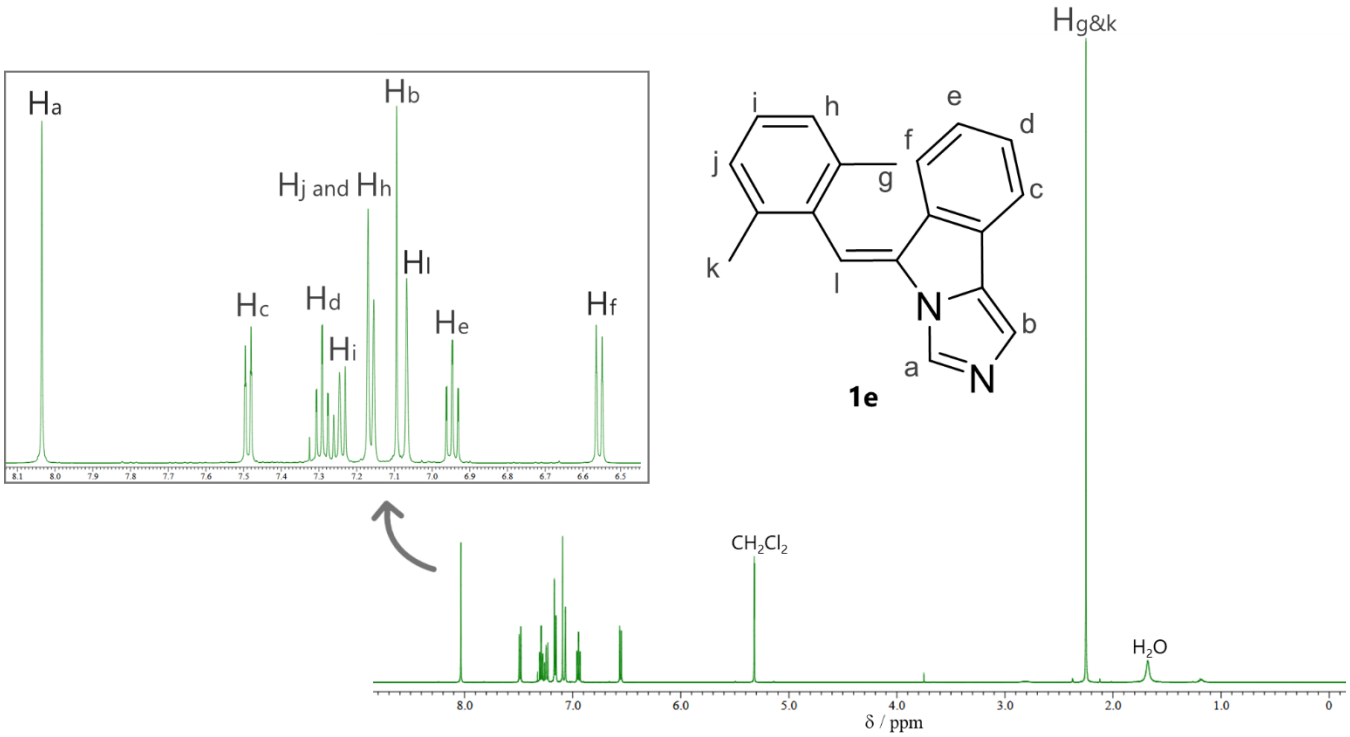

Figure S3. ^{1}H-NMR spectrum of compound **1e**

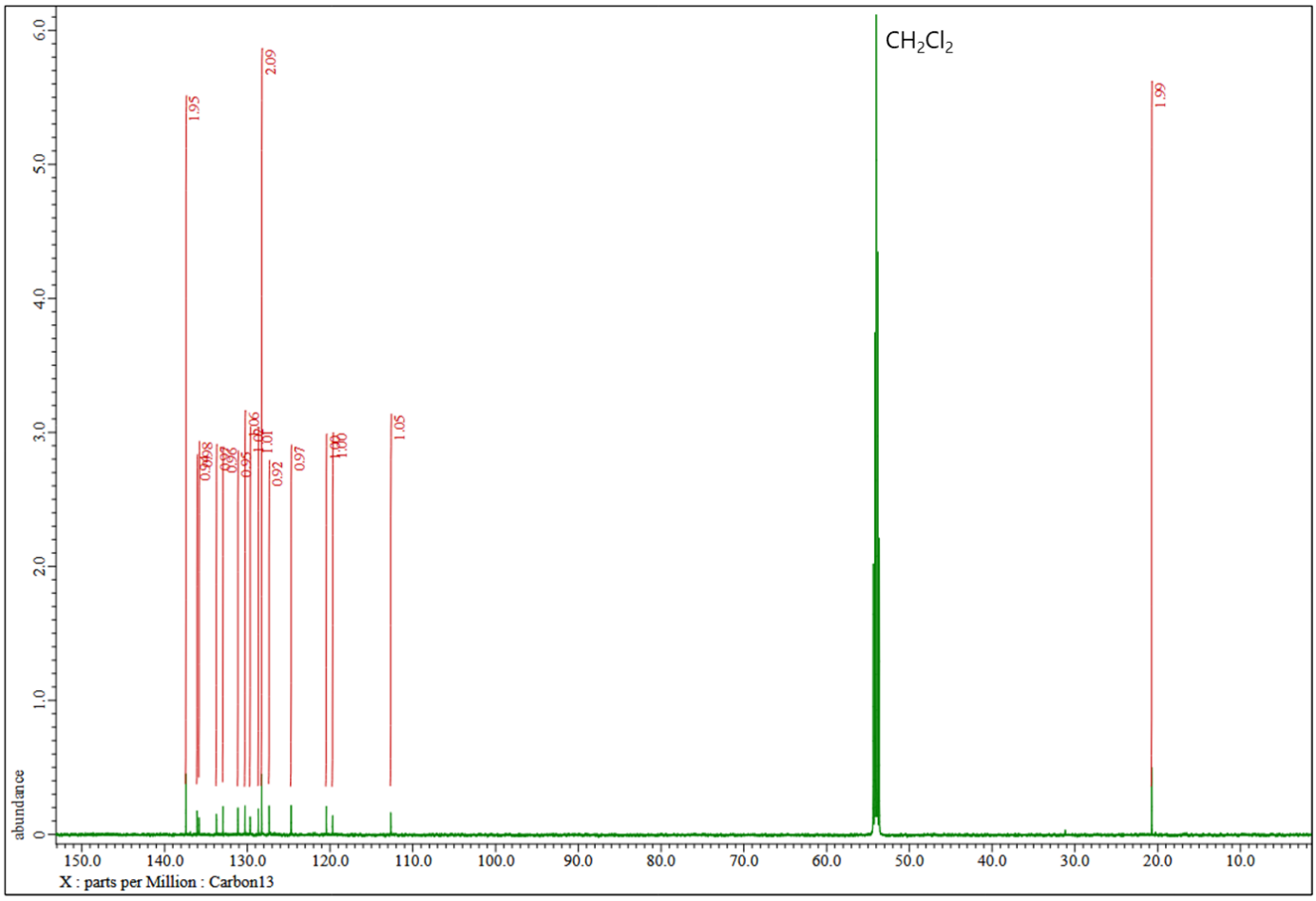

Figure S4. ^{13}C-NMR spectrum of compound **1e**

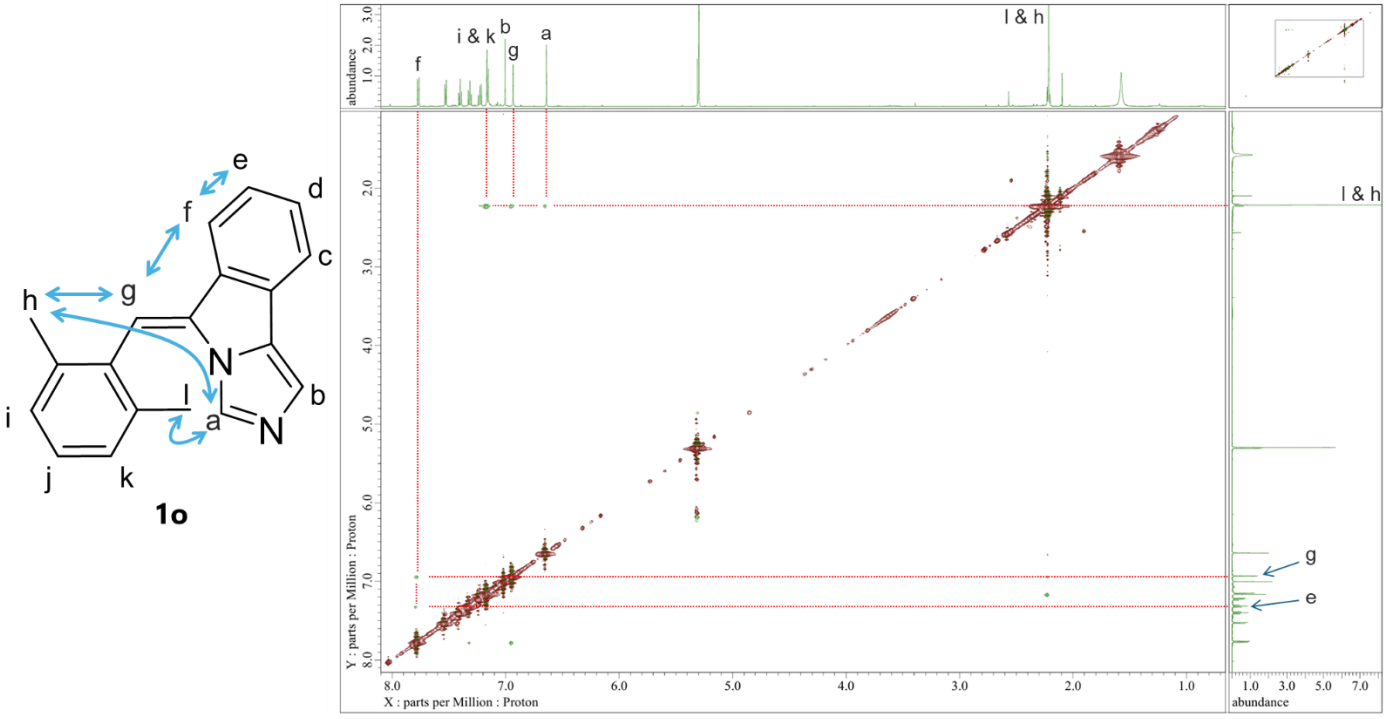

Figure S5. NOESY spectrum of compound **1o** in CD_2Cl_2 at 298 K

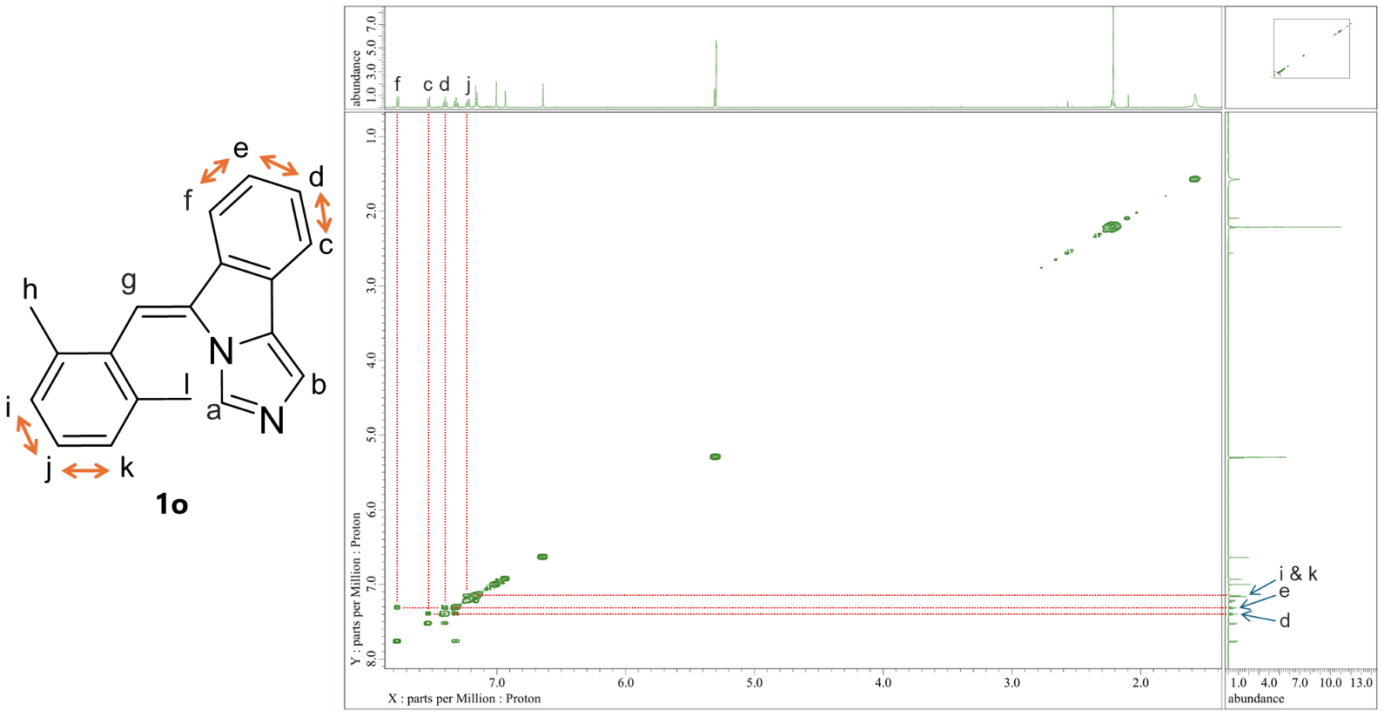

Figure S6 COSY spectrum of compound **1o** in CD_2Cl_2 at 298 K

Compound 7

To a solution of **3** (700 mg, 4.48 mmol, 1.0 eq.) in anhydrous THF (25 mL) at −40° C was added *n*-BuLi(4.0 mL, 6.4 mmol, 1.4 eq., 1.6 M solution hexanes) under Ar. After stirring for 90 min at −40° C, a solution of **6** (0.71 ml, 807 mg, 5.76 mmol, 1.3 eq.) was added and the reaction was allowed to warm to RT overnight and was quenched by adding sat. NH_4Cl aq. The reaction mixture was diluted with water, extracted with CH_2Cl_2 (3 × 100 mL). The combined organic extract was dried overNa_2SO_4 and concentrated under reduced pressure. The crude compound (885 mg) was used in the next reaction without further purification. HRMS (MALDI): *m/z* calcd for $C_{17}H_{17}N_2OS$ +: 297.1056 [M+H]+;found: 297.1059.

Compound 2o and 2e

Compound **7** (crude, 885 mg, 2.99 mmol, 1.0 eq.) was dissolved in anhydrous THF (200 mL) and mixed with methoxy carbonyl sulfamoyl-triethylammonium hydroxide (Burgess reagent; 1.42 g, 5.97 mmol, 2.0eq.). After stirring for 2 h at reflux under Ar, the reaction mixture was washed with sat. aqueous $NaHCO_3$ and extracted with CH_2Cl_2 (3 × 40 mL). The combined organic layers were dried over Na_2SO and concentrated under reduced pressure. The crude was purified by silica-gel column chromatography eluted with MeOH/DCM (1:20) to afford compound **2o** (120.2 mg, 0.43 mmol, 14% yield in two steps) and **2e** (40 mg, 0.143 mmol, 5% yield in two steps).

2o: ^{1}H-NMR (500 MHz, CD_2Cl_2, ppm): δ = 7.66 (d, *J* = 7.0 Hz, 1H; H_f), 7.54 (s, 1H; H_h), 7.50 (d, *J* = 7.7 Hz, 1H; H_c), 7.36 (td, *J* = 7.5, 1.0 Hz, 1H; H_d), 7.26 (td, *J* = 7.6, 1.1 Hz, 1H; H_e), 7.02 (s, 1H; H_b), 6.72 (s, 2H; H_a and H_g), 2.41 (s, 3H; H_i or H_j), 2.31 (s, 3H; H_i or H_j). ^{13}C-NMR (151 MHz, CD_2Cl_2, ppm): δ = 137.8, 137.1, 136.4, 136.1, 132.7, 131.9, 130.6, 129.4, 129.1, 126.6, 124.9, 121.2, 120.0, 118.8, 105.8, 15.1, 13.6. HRMS (MALDI): *m/z* calcd for [$C_{17}H_{14}N_2S$] +: 278.0872 [M]+; found: 278.0872. The molecular structure in the crystal state was determined by single-crystal diffraction analysis. Yellow crystal suitable for SC-XRD were obtained at ambient temperature by liquid-phase slowly diffusion of hexane into a concentrated solution of

the compound in dichloromethane.

2e: ^{1}H-NMR (500 MHz, CD_2Cl_2, ppm): δ = 7.93 (s, 1H; H_a), 7.48 (d, J = 8.4 Hz, 1H; H_c), 7.32 (dd, J = 13.2, 7.7 Hz, 2H; H_f and H_d), 7.09 (td, J = 7.7, 1.1 Hz, 1H; H_e), 7.05 (s, 1H; H_b), 6.90 (s, 1H; H_j), 6.70 (s, 1H; H_i), 2.43 (s, 3H; H_g or H_h), 2.31 (s, 3H; H_i or H_j). ^{13}C-NMR (151 MHz, CD_2Cl_2, ppm): δ = 136.8, 136.0, 135.2, 135.1, 133.0, 130.7, 130.2, 129.7, 128.9, 126.7, 126.3, 124.8, 120.0, 119.2, 108.4, 15.0, 13.8. HRMS (MALDI): *m/z* calcd for [$C_{17}H_{14}N_2S$] +: 278.0872 [M]+; found: 278.0873.

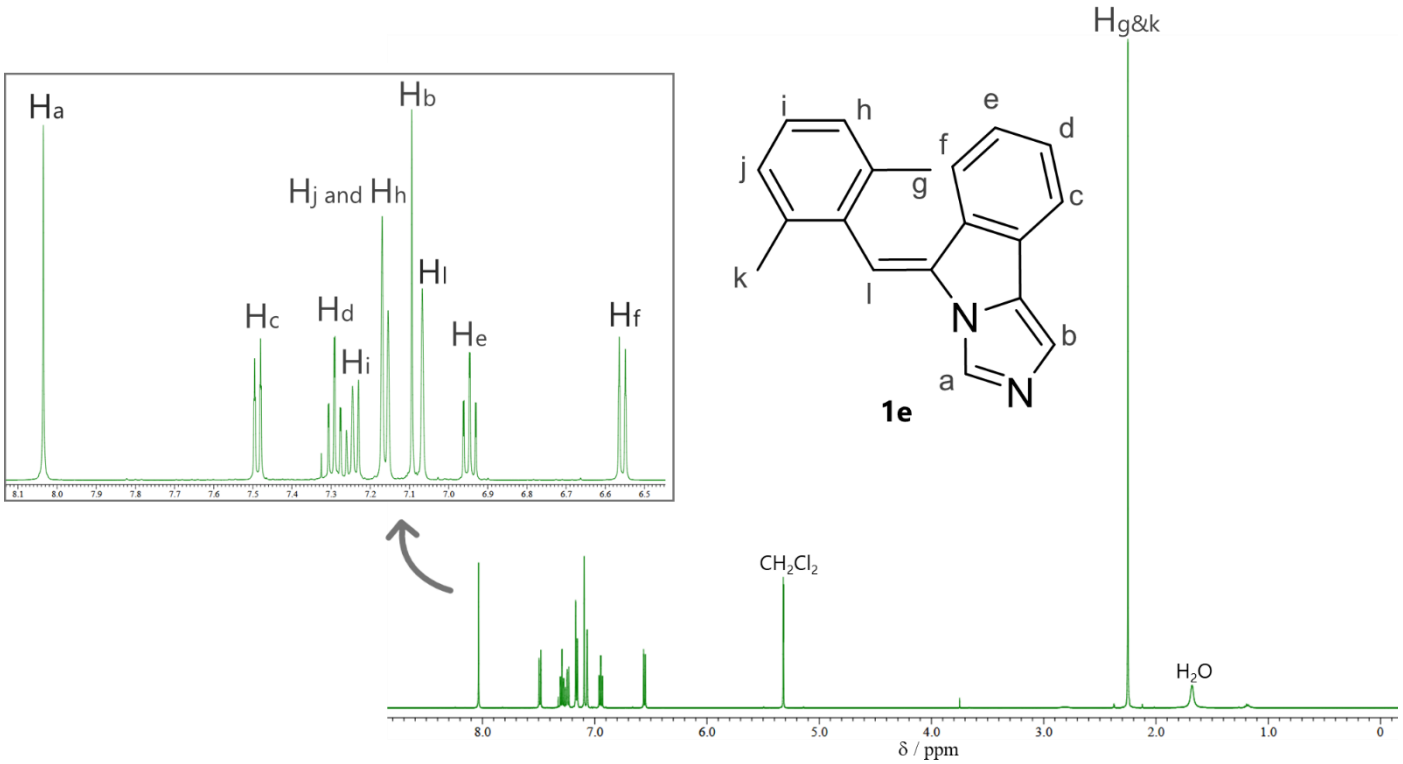

Figure S7. ^{1}H-NMR spectrum of compound **2o**

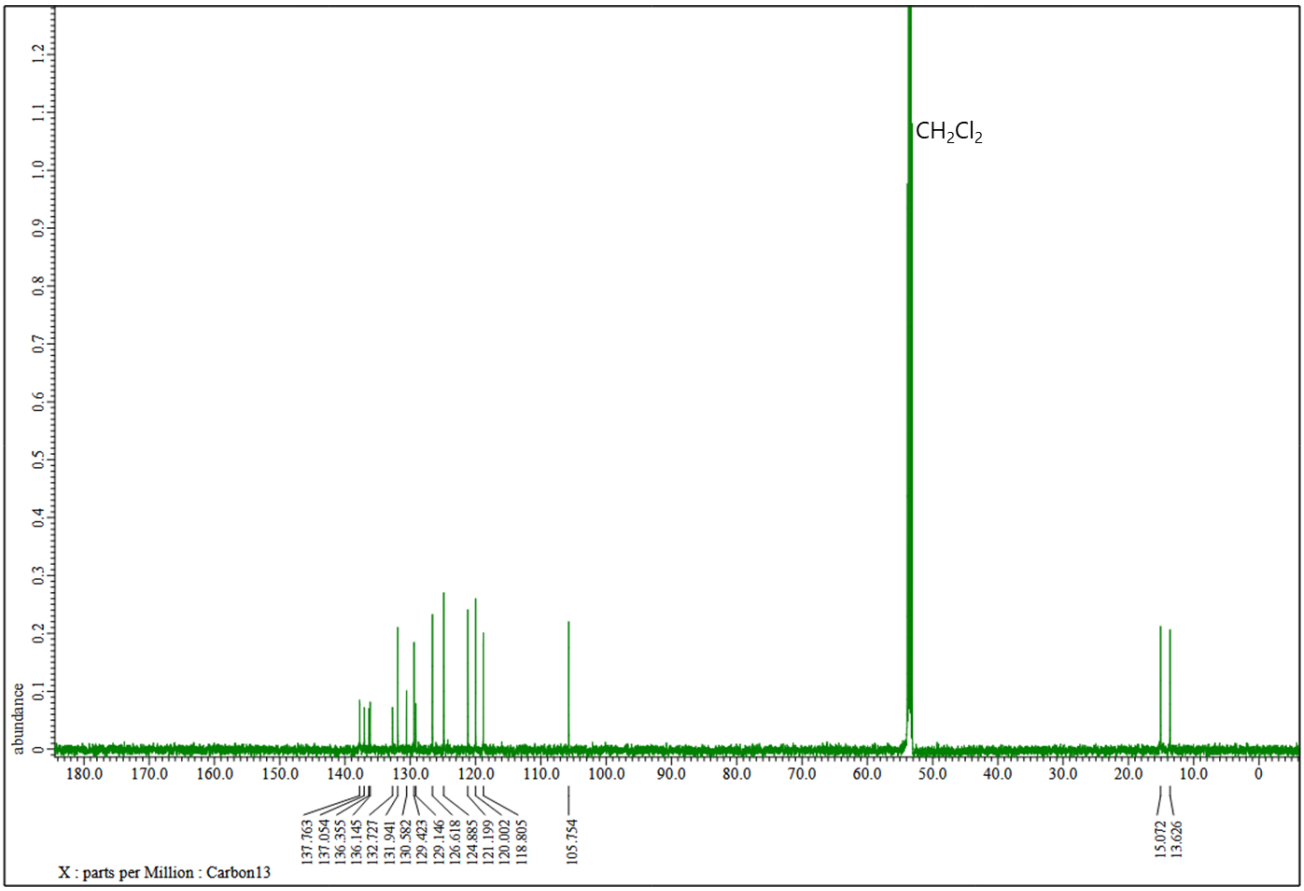

Figure S8. ^{13}C-NMR spectrum of compound **2o**

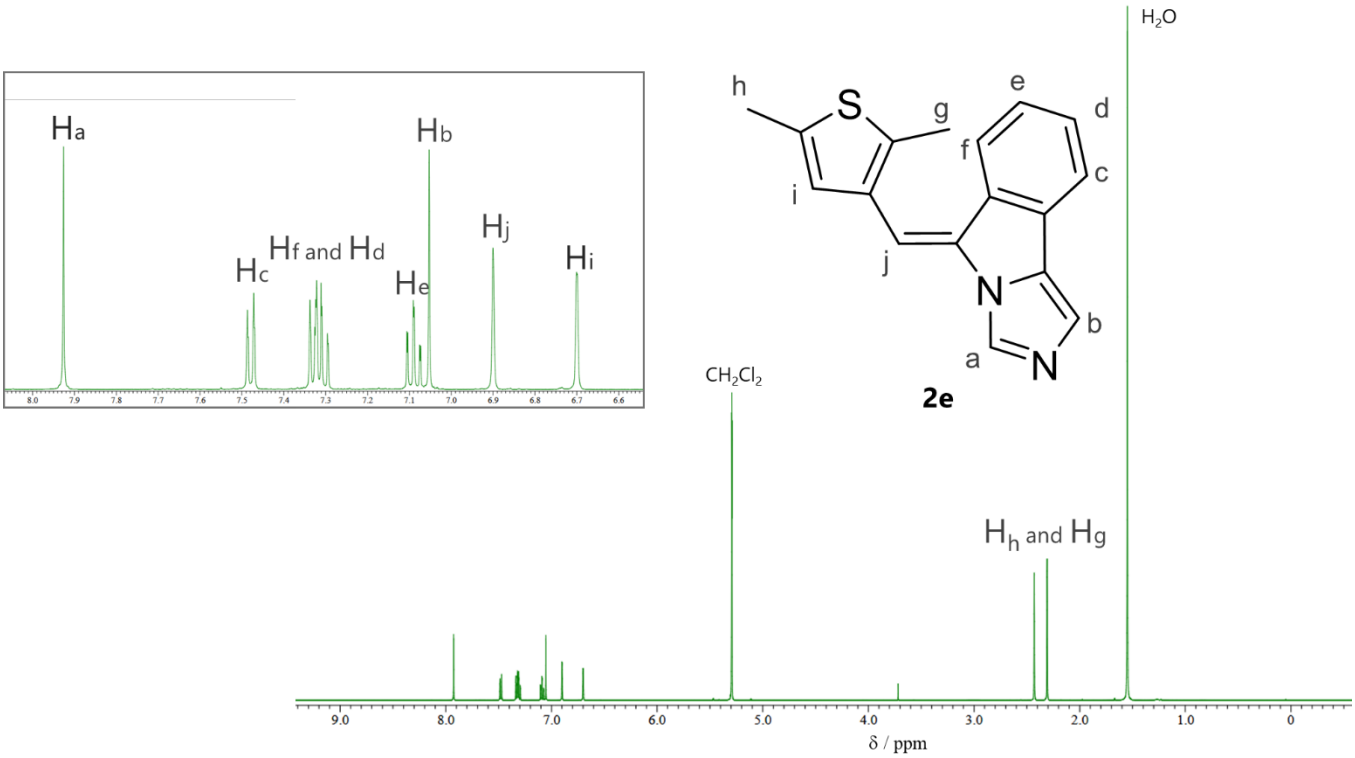

Figure S9. ^{1}H-NMR spectrum of compound **2e**

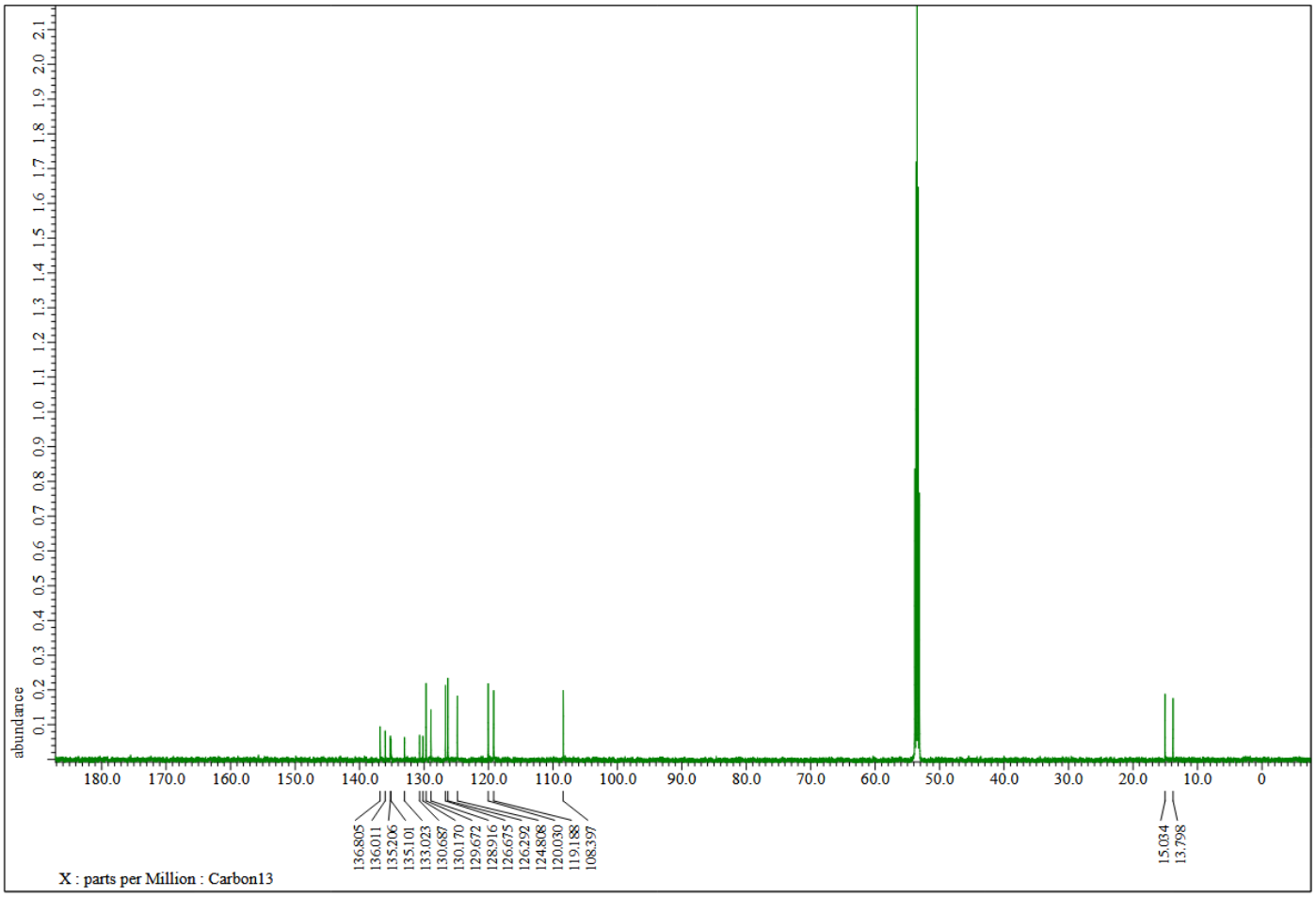

Figure S10. ^{13}C-NMR spectrum of compound **2e**

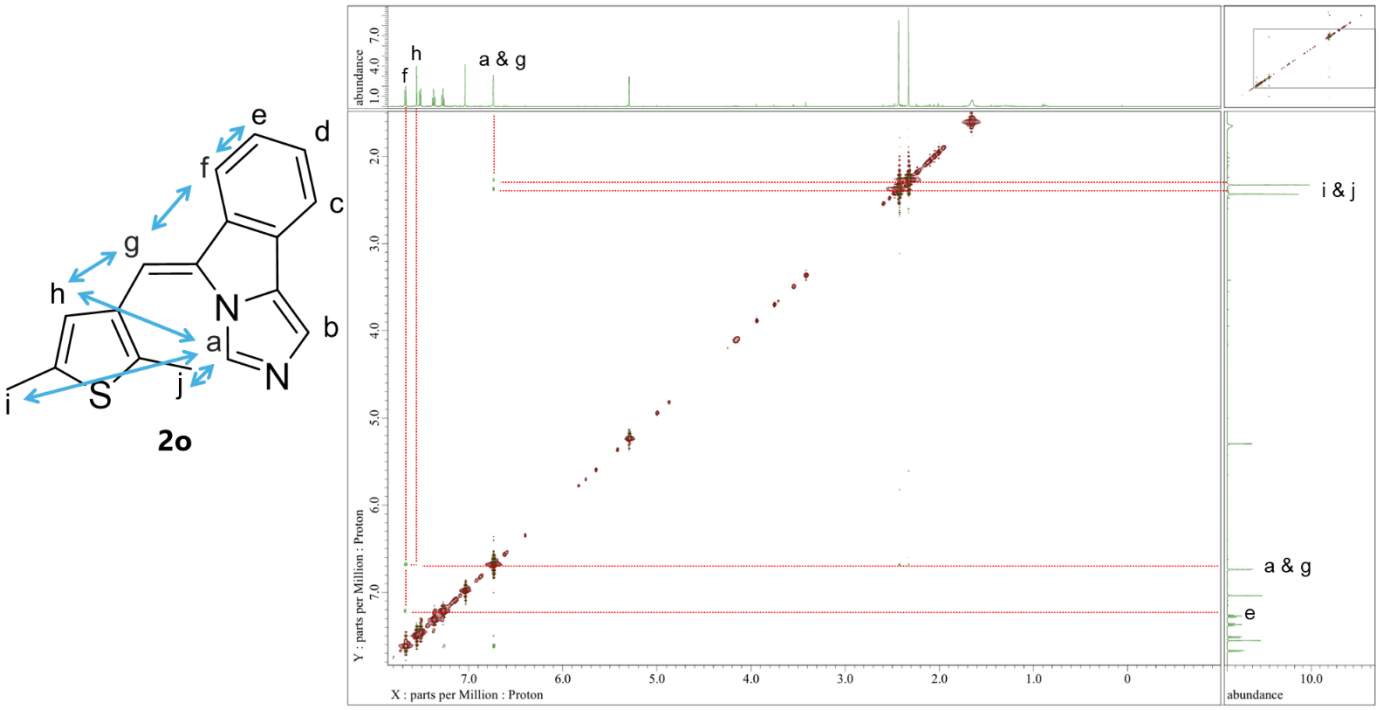

Figure S11. NOESY spectrum of compound **2o** in CD_2Cl_2 at 298 K

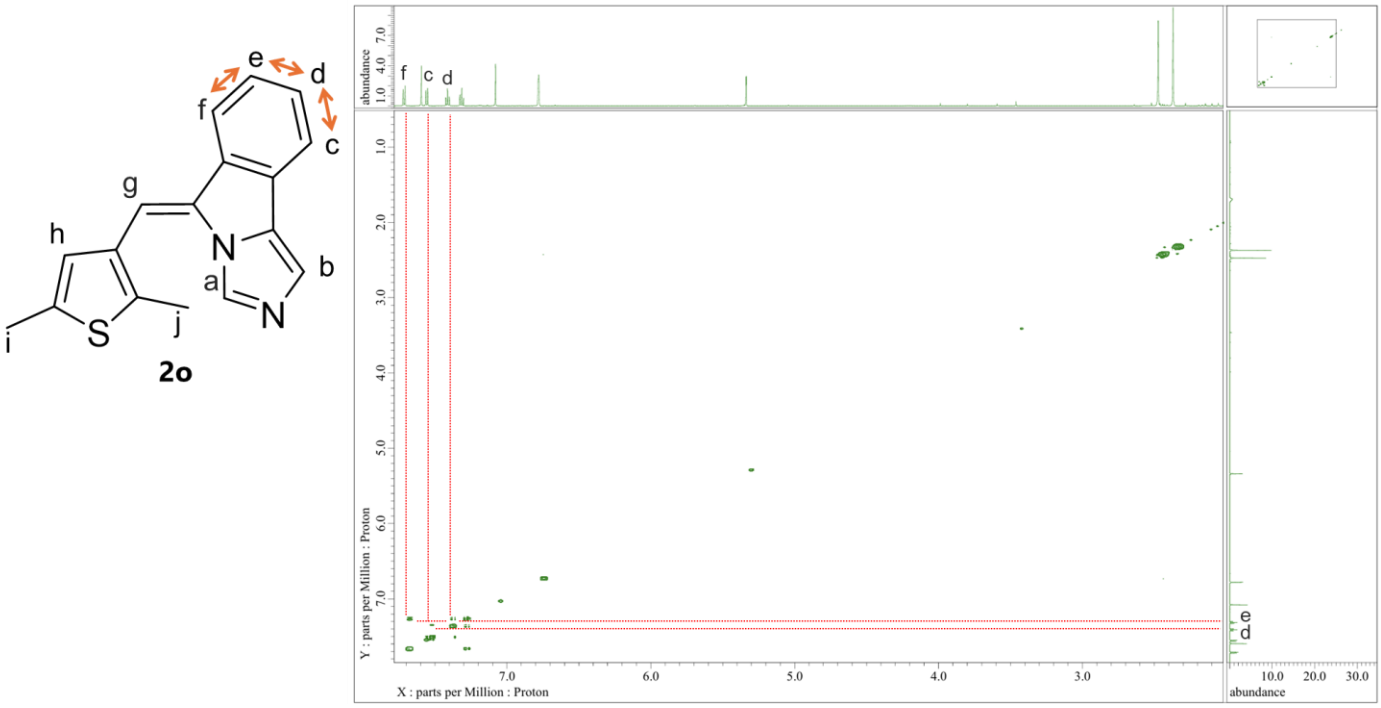

Figure S12. COSY spectrum of compound **2o** in CD_2Cl_2 at 298 K

3. X-ray crystallographic analysis

Table S1. Crystallographic data for **1o** and **2o**.

	1o	**2o**
Formula	$C_{19}H_{16}N_2$	$C_{17}H_{14}N_2S$
Formula weight	272.34	278.36
T/K	103.00(10)	103.00(10)
Crystal system	Monoclinic	Monoclinic
Space group	P21/c	P21/c
a/Å	23.5932(2)	18.6058(2)
b/Å	8.13930(10)	5.13880(10)
c/Å	15.3079(2)	14.6790(2)
α/°	90	90
β/°	104.6980	104.3770
γ/°	90	90
V/Å^3	2843.41(6)	1359.5(4)
Z	8	4
Density / g cm^3	1.272	1.360
Goodness-of-fit on F^2	1.041	1.101
R_1 ($I > 2\sigma(I)$)	0.0361	0.0449
wR_2 ($I > 2\sigma(I)$)	0.0902	0.1252
R_1 (all data)	0.0375	0.0462
wR_2 (all data)	0.0913	0.1263
CCDC No.	2481797	2481798

4. TD-DFT calculation

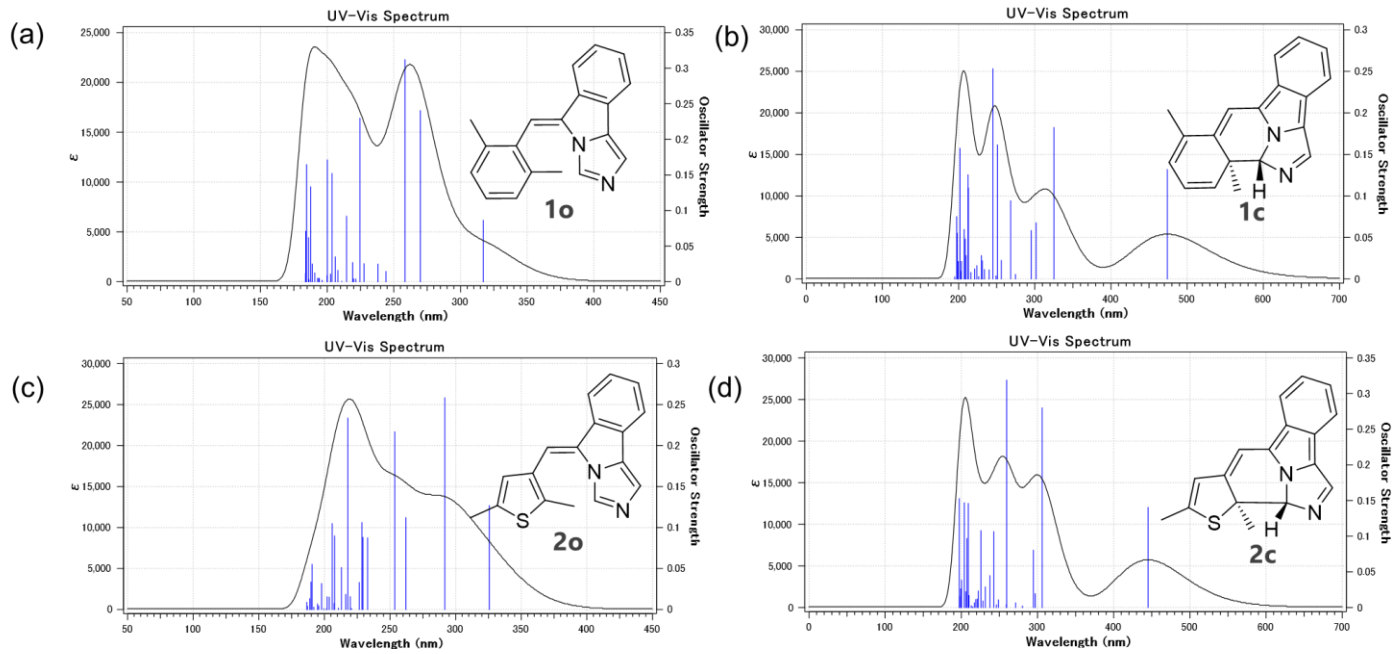

Figure S13. Calculated UV-vis spectra of (a) **1o**, (b) **1c**, (c) **2o**, and (d) **2c** (black) with oscillator strength values (blue), Calculation level: M062x/6–311 + G(d,p)

5. Photoswitching cycle

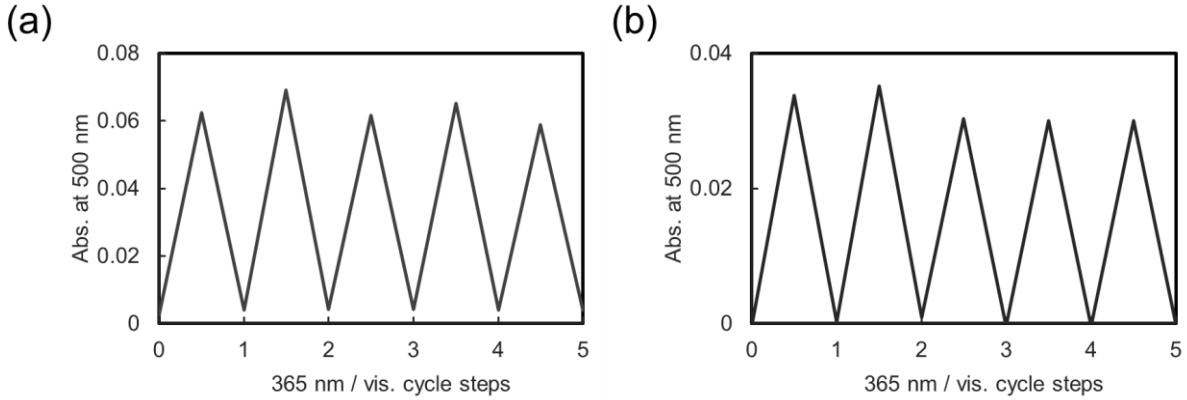

Figure S14. Photoswitching cycle: (a)**1o**/**1c**, (b)**2o**/**2c**

6. Photochromism in Acetonitrile

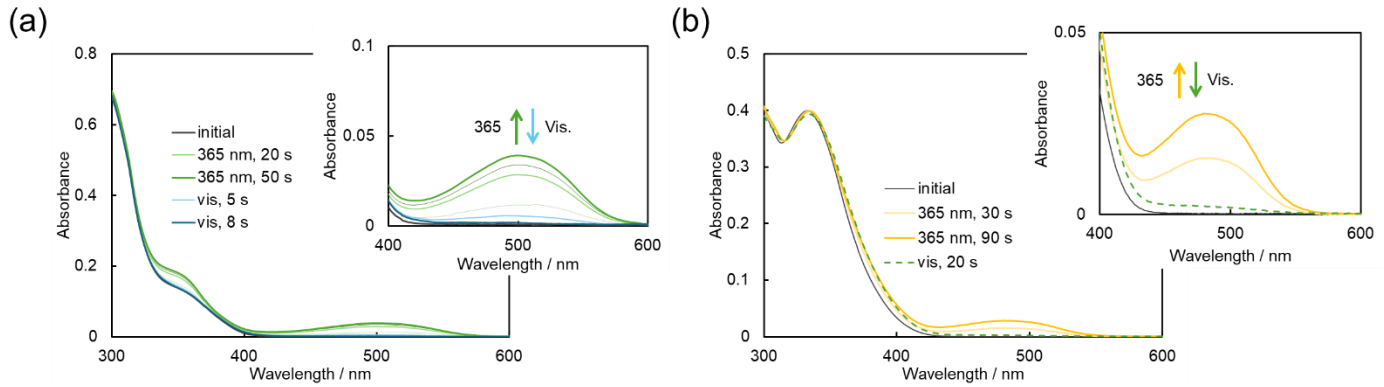

Figure 15. Absorption spectral changes in MeCN of (a) **1o** (6.4×10^{-5} M) and (b) **2o** (3.8×10^{-5} M).

7. Spectroscopic properties

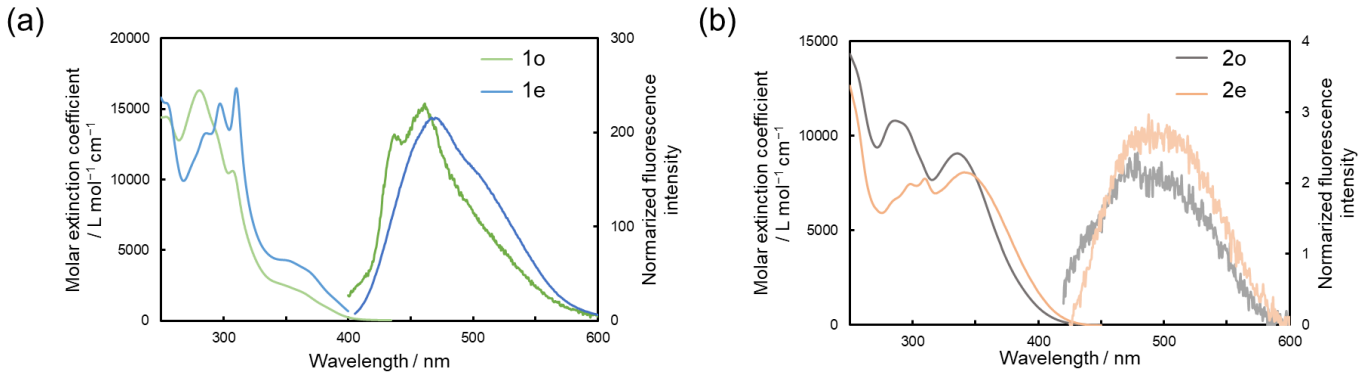

Figure S16. Absorption and emission spectra of (a) **1o**/**1e** and (b) **2o**/**2e** in CH_2Cl_2. Excitation wavelengths: 280 nm for **1o**, 310 nm for **1e**, 290 nm for **2o**, and 345 nm for **2e**.

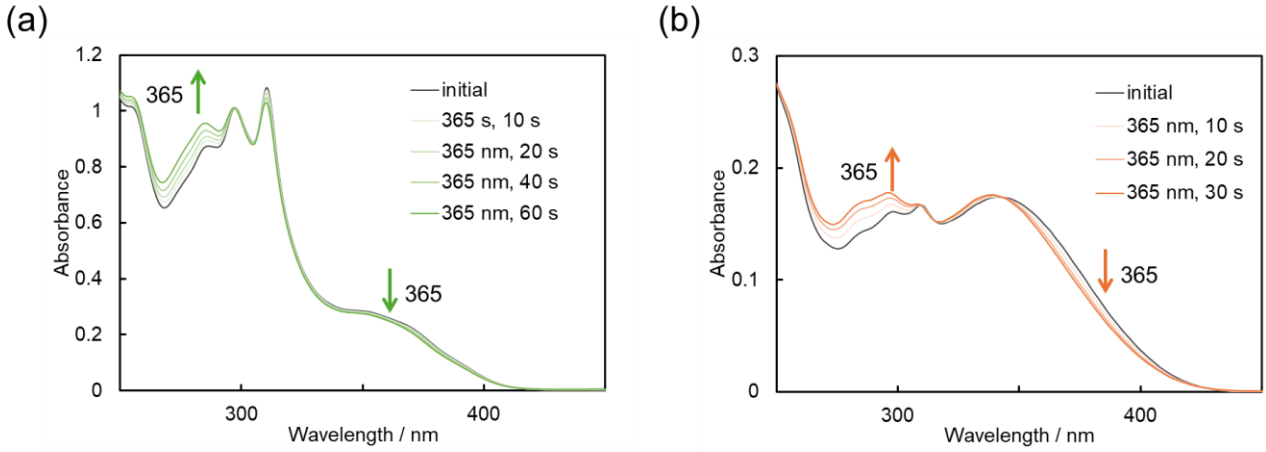

Figure 17. Absorption spectral changes in CH_2CH_2 of (a) **1e** (5.9×10^{-5} M) and (b) **2e** (2.2×10^{-5} M).

Table S2. Emission quantum yields of **1o**/**1e** and **2o**/**2e** in CH_2Cl_2. Excitation wavelengths: 280 nm for **1o**, 310 nm for **1e**, 290 nm for **2o**, and 345 nm for **2e**. (a) Samples were bubbled with Ar gas for 5 minutes.

	ϕ_f (Air) [%]	ϕ_f (Ar)[a][%]
1o	4.3	4.7
1e	14	16
2o	1.7	1.7
2e	1.1	1.3

8. ^{1}H-NMR tracking

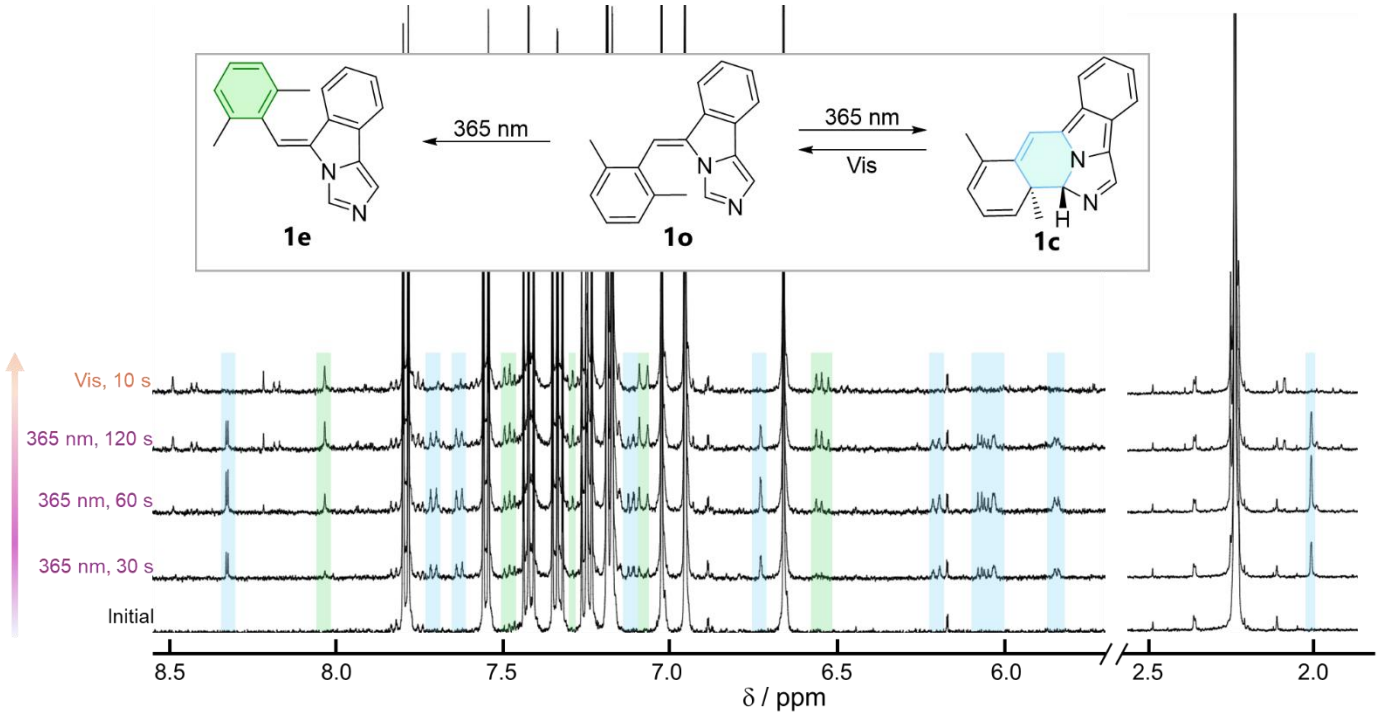

Figure 18. ^{1}H-NMR spectral changes of **1o** (500 MHz, CD_2Cl_2) before and after light irradiation. **1c** (blue) and **1e** (green).

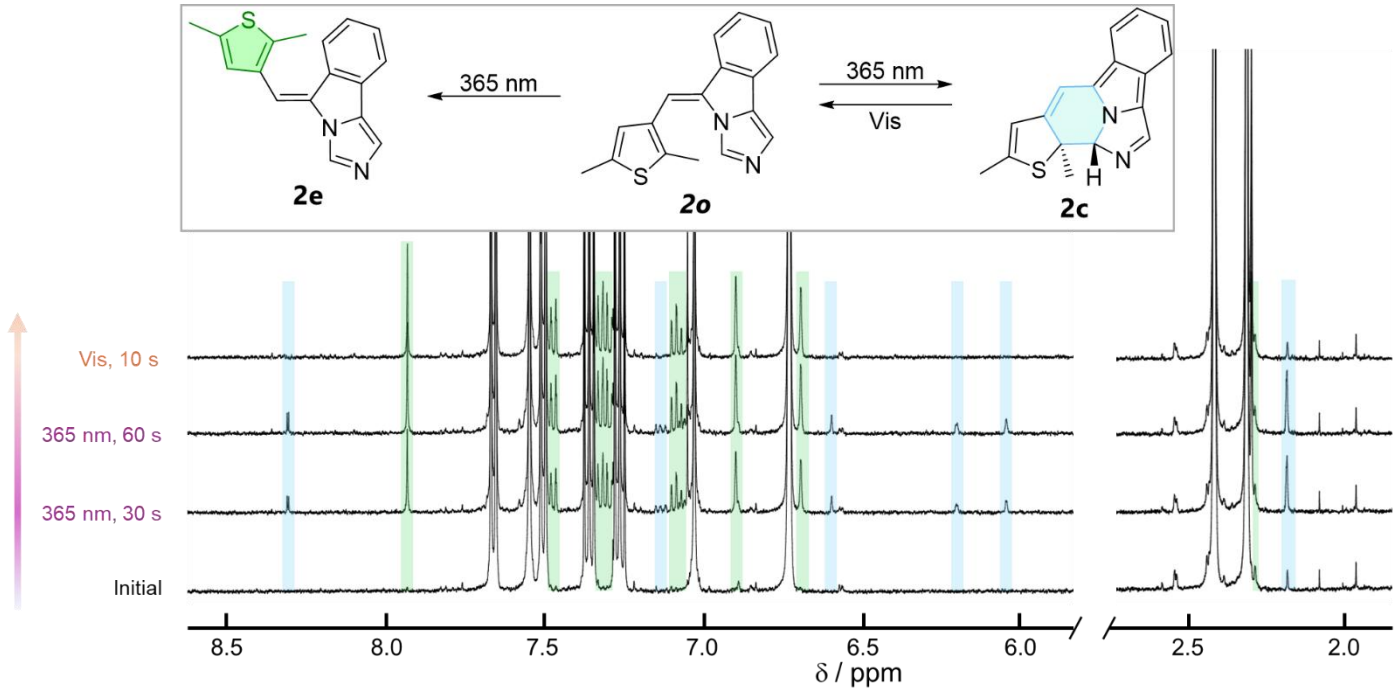

Figure 19. ^{1}H-NMR spectral changes of **2o** (500 MHz, CD_2Cl_2) before and after light irradiation. **2c** (blue) and **2e** (green).

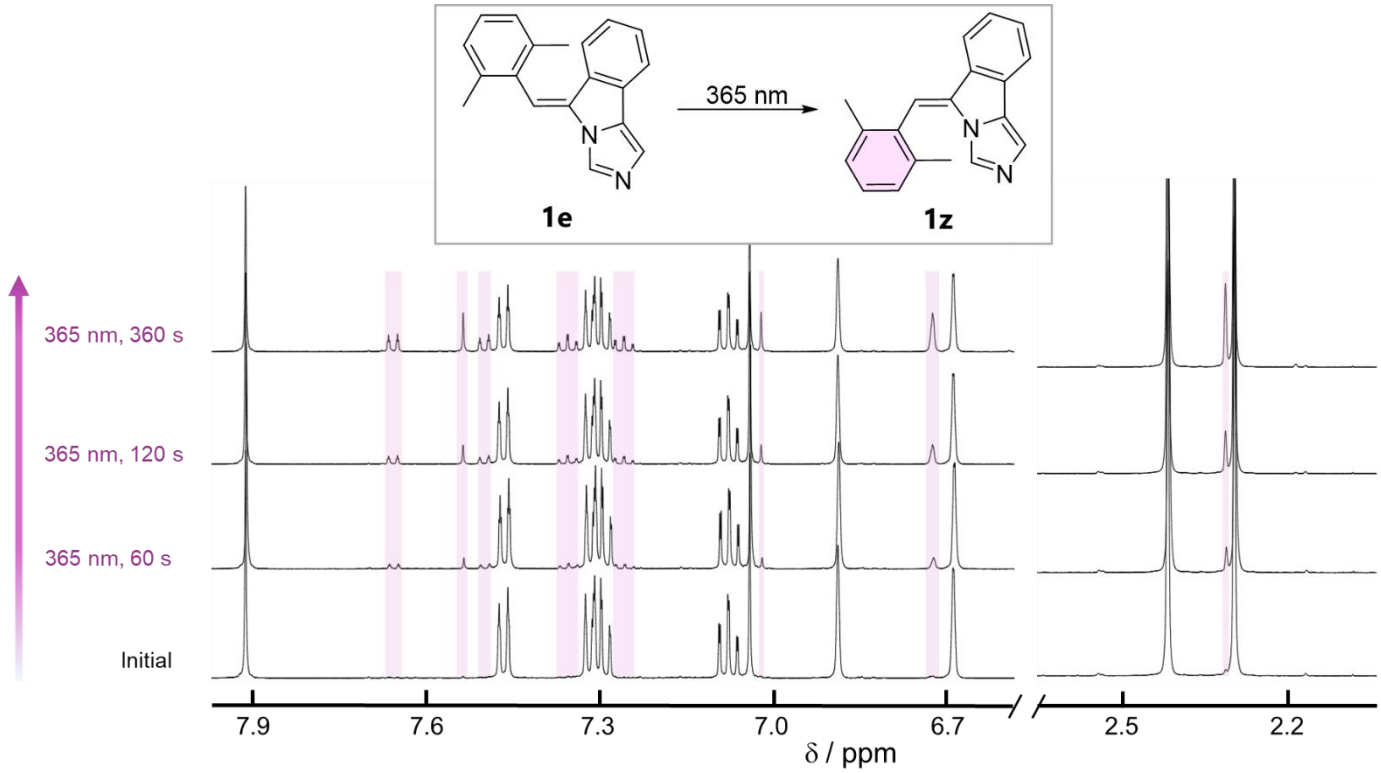

Figure 20. ^{1}H-NMR spectral changes of **1e** (500 MHz, CD_2Cl_2) before and after light irradiation. **1e** (pink).

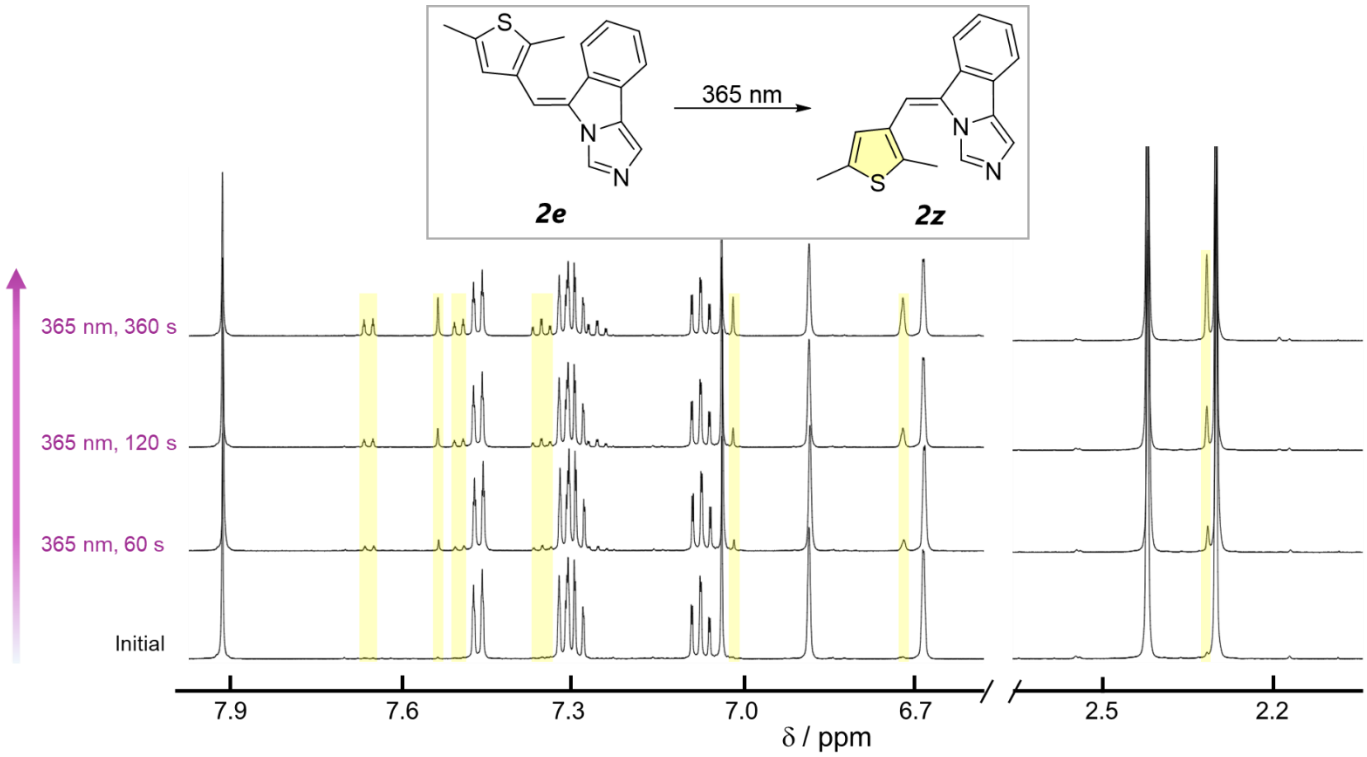

Figure 21. ^{1}H-NMR spectral changes of **2e** (500 MHz, CD_2Cl_2) before and after light irradiation. **2e** (yellow).

9. Activation Energy Determination

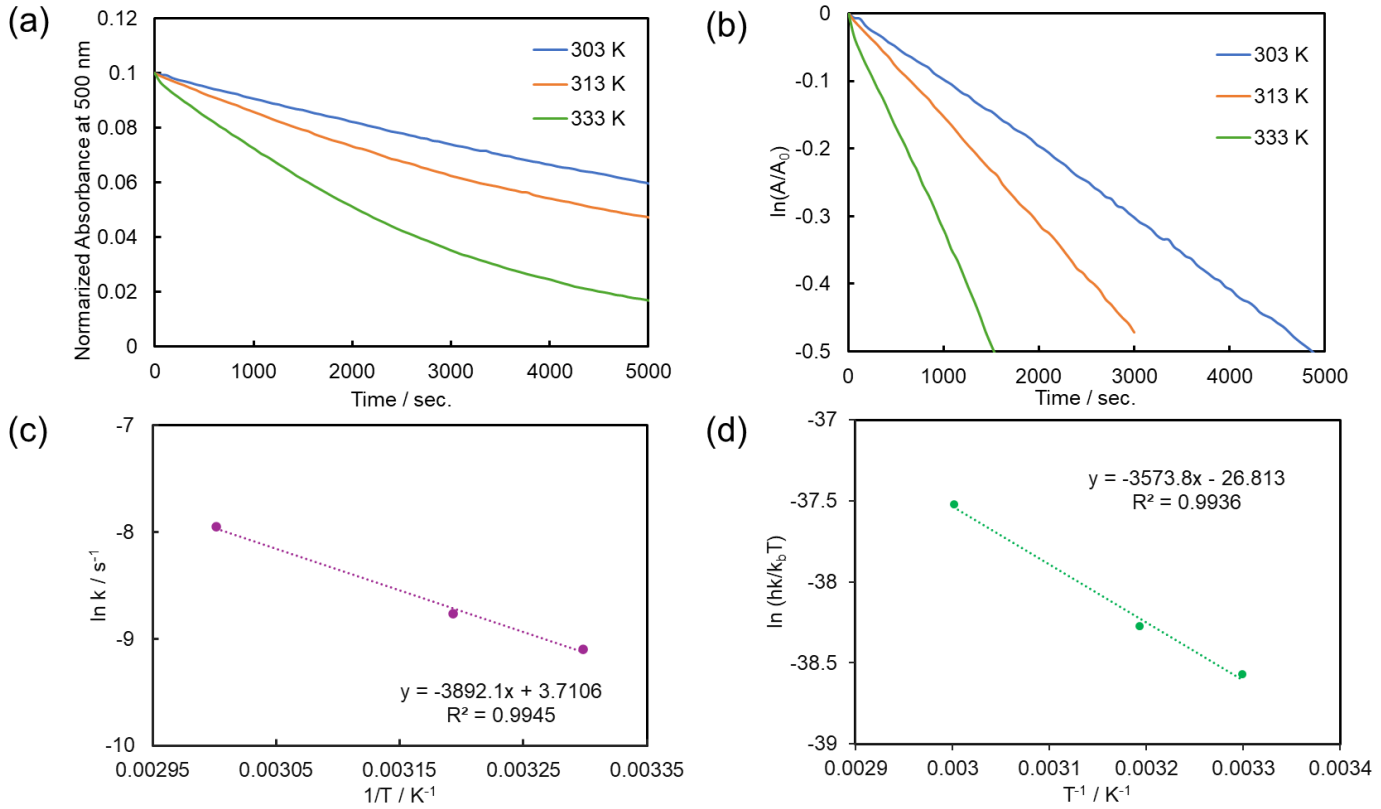

Figure S22. (a) Decay time profiles of the cycloreversion after photoirradiation of **1c** in toluene at various temperatures; (b) First-order plots of absorbance decay at 500 nm. Slopes ($\times 10^{-3}$) and correlation coefficients (R^2) were –0.112 (303 K, 0.999), –0.156 (313 K, 0.999), and –0.351 (333 K, 0.999); (c) Arrhenius plot with activation parameters Ea = 32 kJ mol^{-1} and A = 41 s^{-1}; (d) Eyring plot with $\Delta H^{\ddagger}$ = 30 kJ mol^{-1} and $\Delta S^{\ddagger}$ = –223 J K^{-1} mol^{-1}.

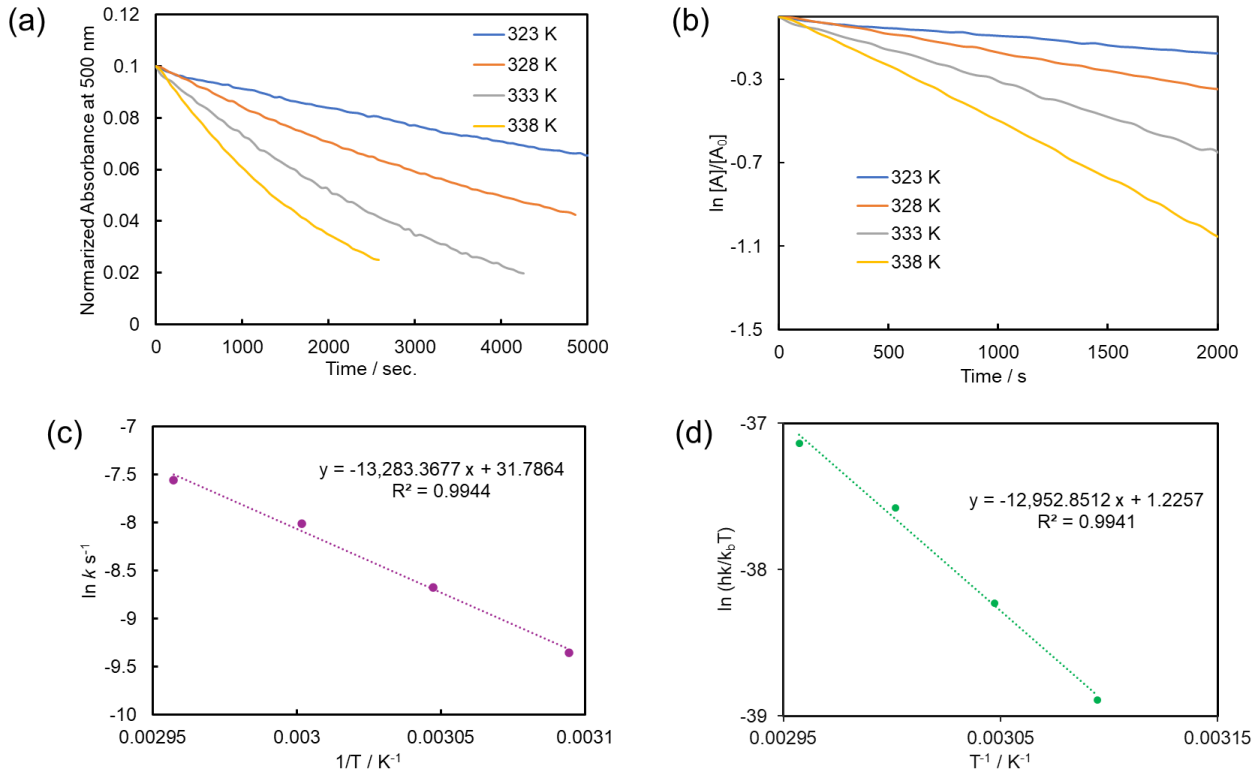

Figure S23. (a) Decay time profiles of the cycloreversion after photoirradiation of **2c** in toluene at various temperatures; (b) First-order plots of absorbance decay at 500 nm. Slopes ($\times 10^{-3}$) and correlation coefficients (R^2) were –0.0865 (323 K, 0.999), –0.171 (328 K, 0.999), –0.330 (333 K, 0.999), and –0.525 (338 K, 0.999); (c) Arrhenius plot with activation parameters Ea = 110 kJ mol^{-1} and A = 6.1×10^{13} s^{-1}; (d) Eyring plot with $\Delta H^{\ddagger}$ = 108 kJ mol^{-1} and $\Delta S^{\ddagger}$ = 10 J K^{-1} mol^{-1}.

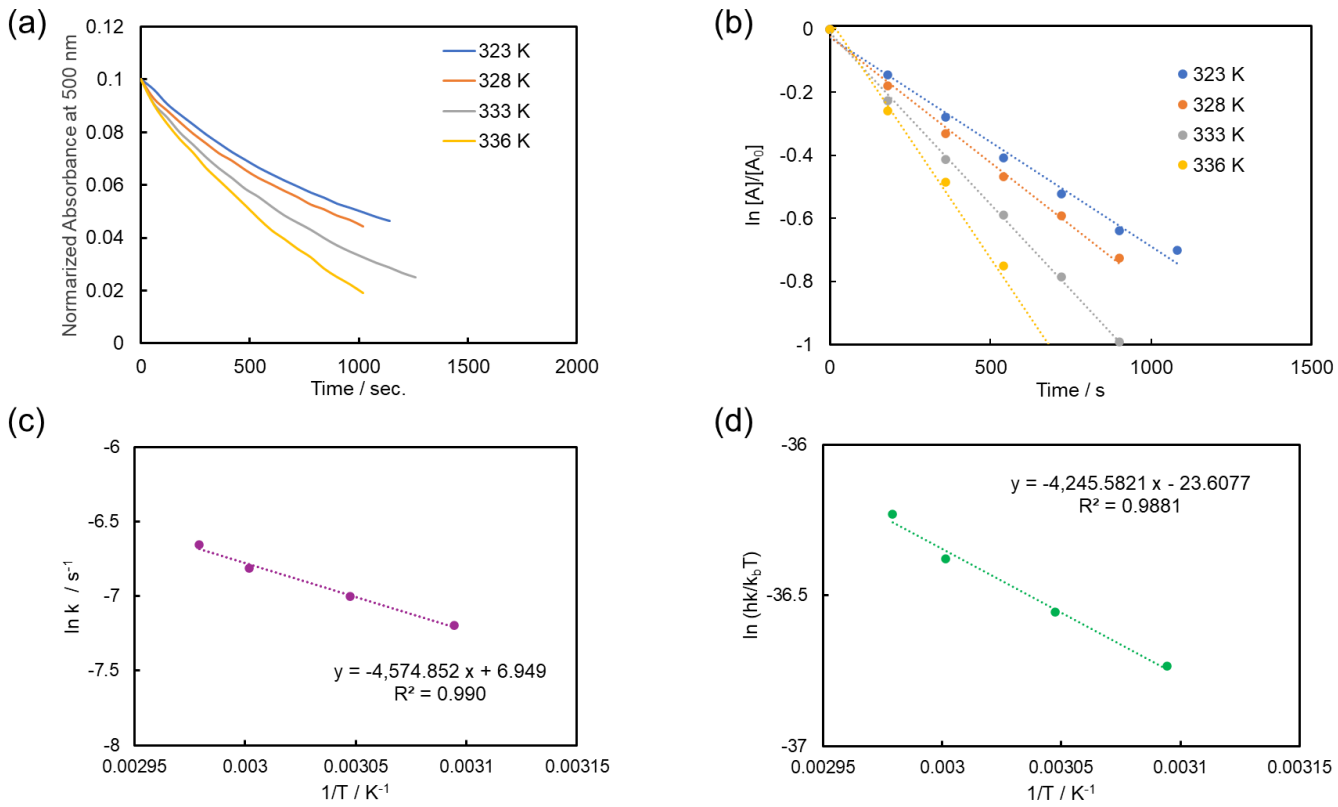

Figure 24. (a) Decay time profiles of the cycloreversion after photoirradiation of **1c** in MeCN at various temperatures; (b) First-order plots of absorbance decay at 500 nm. Slopes ($\times 10^{-3}$) and correlation coefficients (R^2) were –0.749 (323 K, 0.999), –0.910 (328 K, 0.997), –1.10 (333 K, 0.999), and –1.36 (336 K, 0.999); (c) Arrhenius plot with activation parameters Ea = 41 kJ mol^{-1} and A = 3200 s^{-1}; (d) Eyring plot with $\Delta H^{\ddagger}$ = 35 kJ mol^{-1} and $\Delta S^{\ddagger}$ = –187 J K^{-1} mol^{-1}.

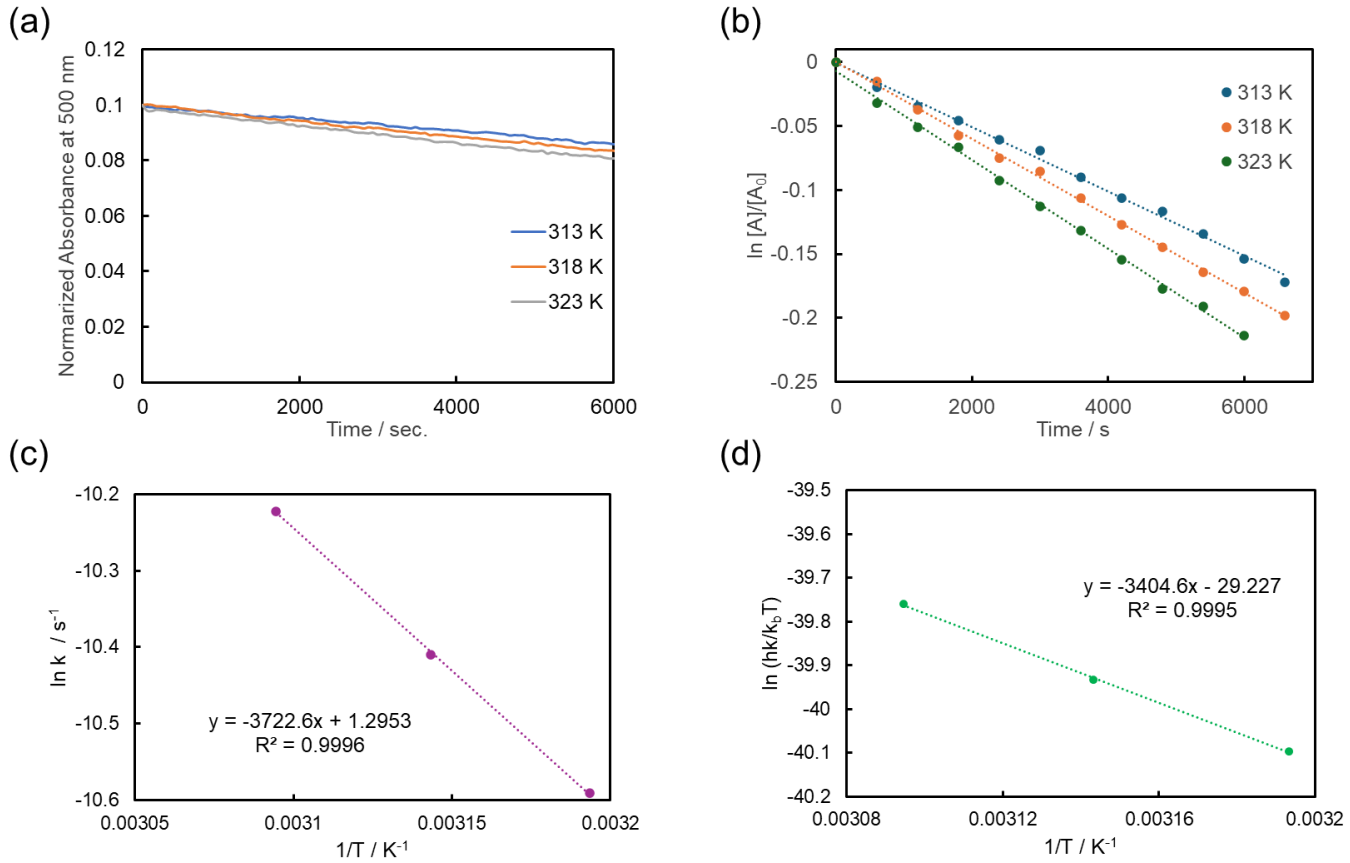

Figure S25. (a) Decay time profiles of the cycloreversion after photoirradiation of 2c in MeCN at various temperatures; (b) First-order plots of absorbance decay at 500 nm. Slopes ($\times 10^{-3}$) and correlation coefficients (R^2) were –0.0252 (313 K, 0.998), –0.0301 (318 K, 0.999), and –0.0364 (323 K, 0.998); (c) Arrhenius plot with activation parameters Ea = 31 kJ mol^{-1} and A = 3.7 s^{-1}; (d) Eyring plot with $\Delta H^{\ddagger}$ = 28 kJ mol^{-1} and $\Delta S^{\ddagger}$ = –243 J K^{-1} mol^{-1}.

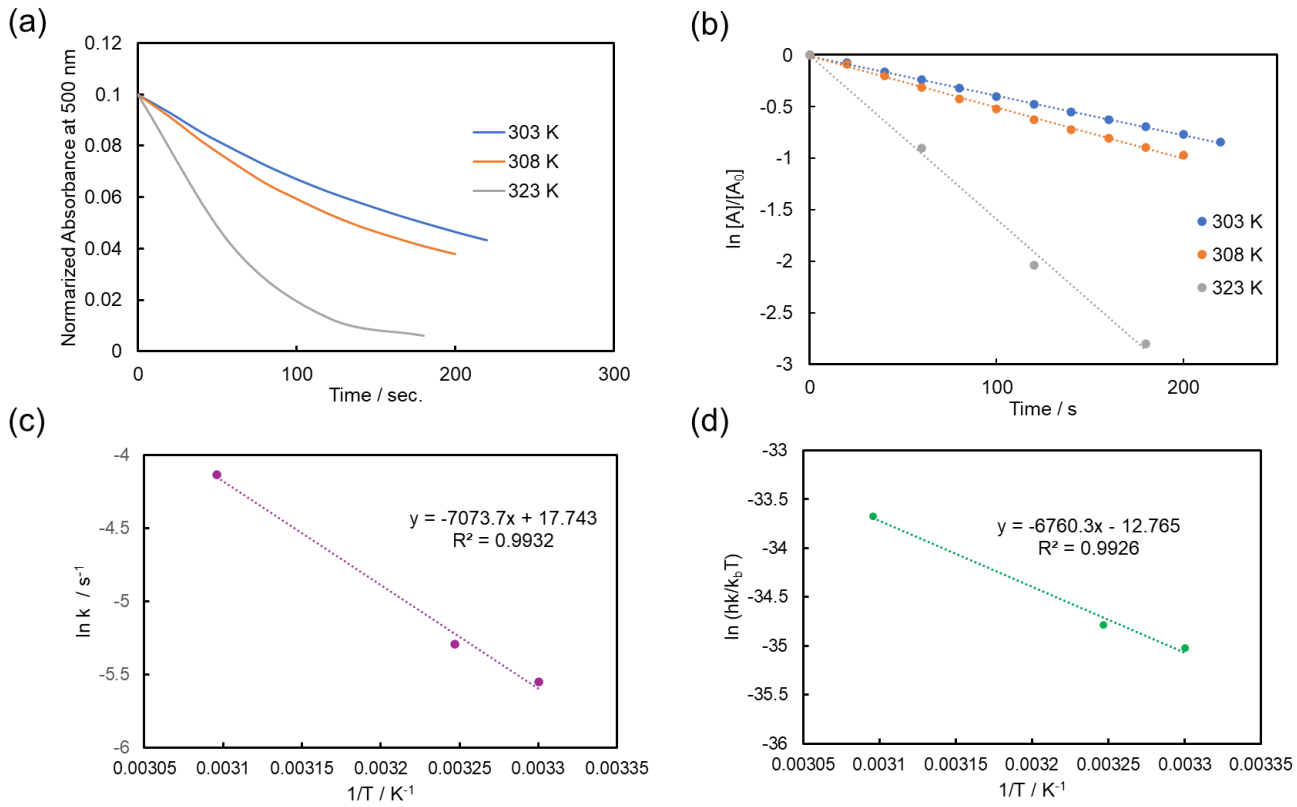

Figure S26. (a) Decay time profiles of the cycloreversion after photoirradiation of 1c in MeCN under acidic conditions (TFA, 5 eq.) at various temperatures; (b) First-order plots of absorbance decay at 500 nm. Slopes ($\times 10^{-3}$) and correlation coefficients (R^2) were –3.88 (303 K, 0.999), –5.03 (308 K, 0.999), and –15.9 (323 K, 0.998); (c) Arrhenius plot with activation parameters Ea = 59 kJ mol^{-1} and A = 5.1 $\times 10^7$ s^{-1}; (d) Eyring plot with $\Delta H^{\ddagger}$ = 56 kJ mol^{-1} and $\Delta S^{\ddagger}$ = –106 J K^{-1} mol^{-1}.

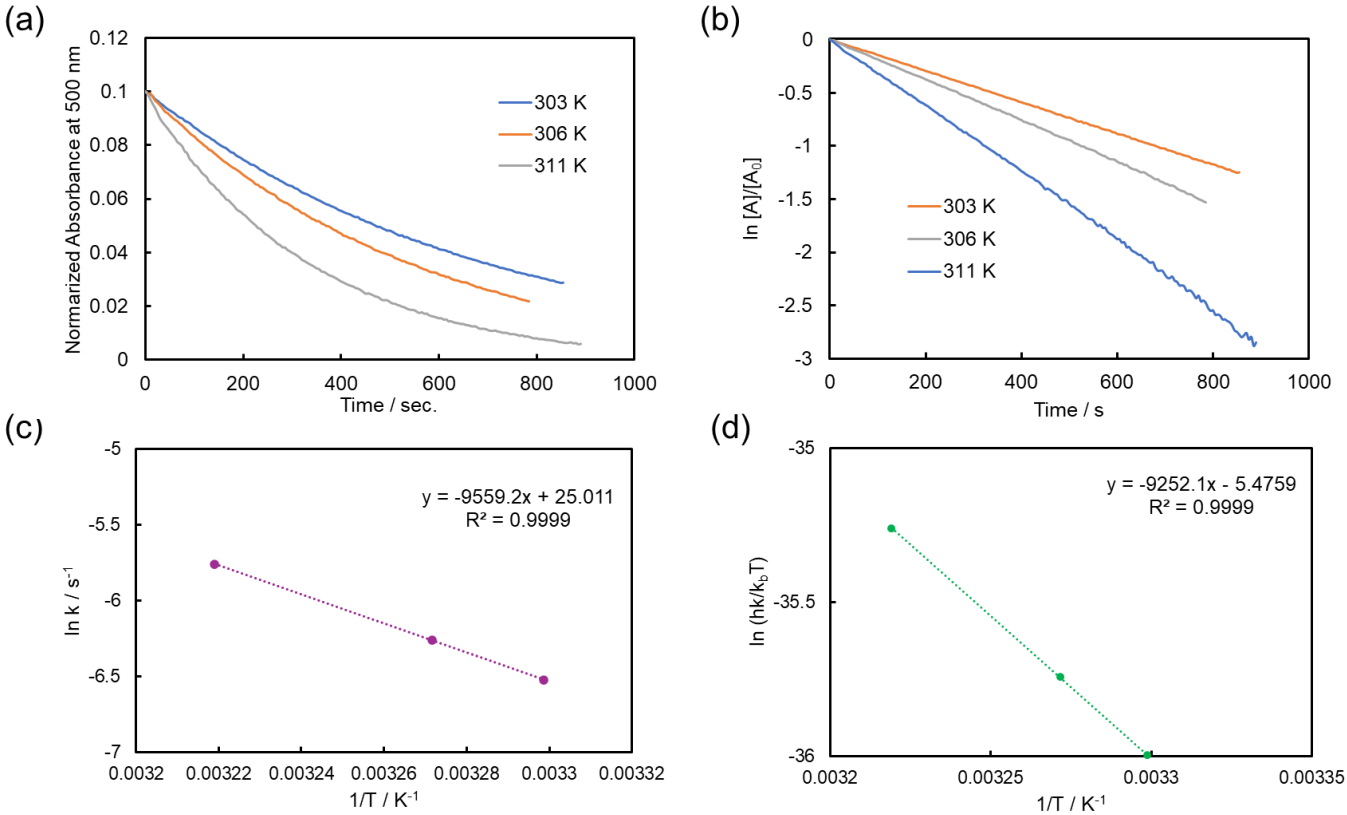

Figure S27. (a) Decay time profiles of the cycloreversion after photoirradiation of **2c** in MeCN under acidic conditions (TFA, 5 eq.) at various temperatures; (b) First-order plots of absorbance decay at 500 nm. Slopes ($\times 10^{-3}$) and correlation coefficients (R^2) were –1.47 (303 K, 0.999), –1.91 (306 K, 0.999), and –3.15 (311 K, 0.999); (c) Arrhenius plot with activation parameters Ea = 80 kJ mol^{-1} and A = 7.3 $\times 10^{10}$ s^{-1}; (d) Eyring plot with $\Delta H^{\ddagger}$ = 77 kJ mol^{-1} and $\Delta S^{\ddagger}$ = –46 J K^{-1} mol^{-1}.

10. Acidic titration

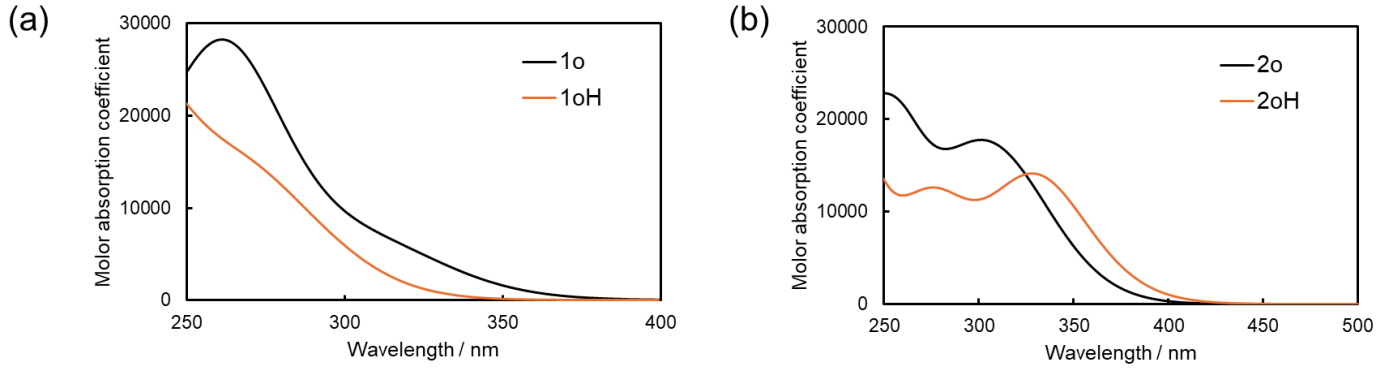

Figure S28. Calculated UV–vis spectra of (a) **1o** and **1oH** and (b) **2o** and **2oH**. Calculations were performed at the M06-2X/6-311+G(d,p) level using the IEFPCM solvation model with dichloromethane as the solvent.

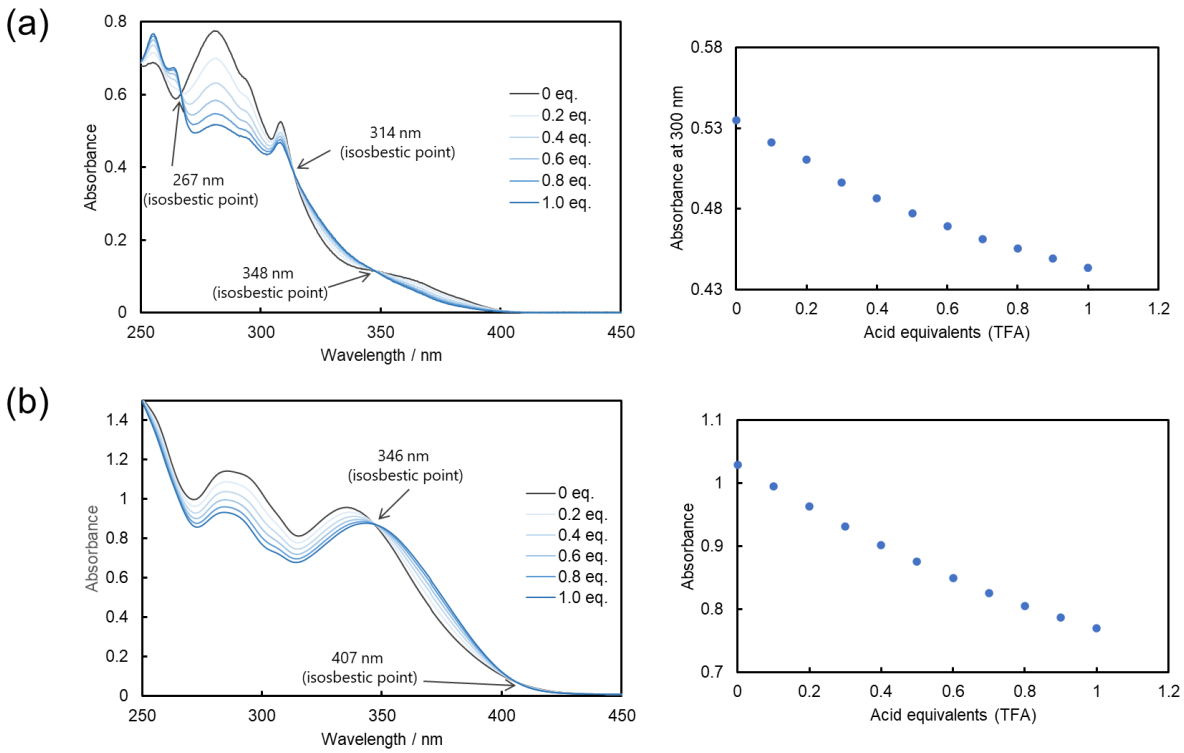

Figure S29. UV-visible spectral change and titration curve in CH_2Cl_2 (black to blue solid lines) during the acidic titration of (a) **1o** (4.6×10^{-5} M) and (b) **2o** (1.0×10^{-4} M).

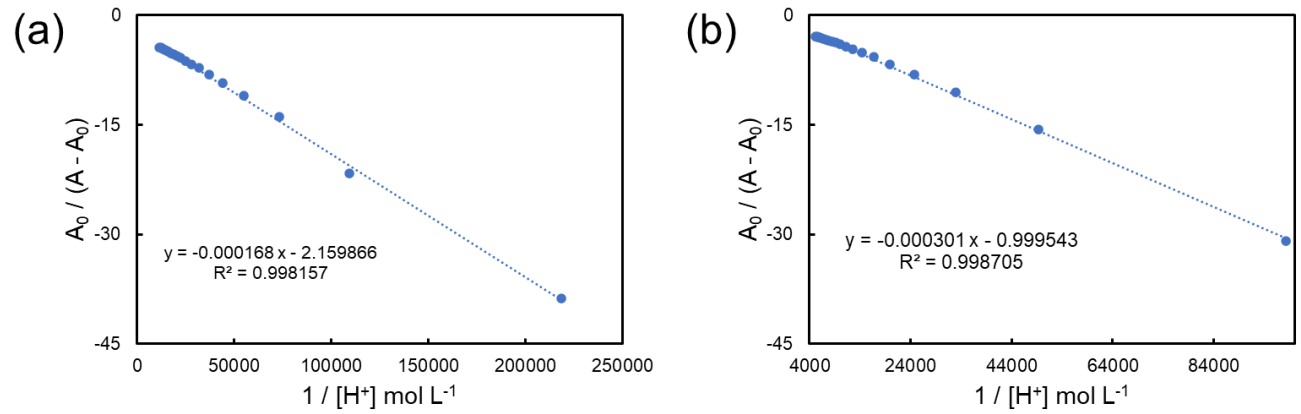

Figure S30. Plots for determining the association constants of (a) **1o** ($K_a = 1.3 \times 10^4$ mol^{-1} L) and (b) **2o** ($K_a = 3.3 \times 10^3$ mol^{-1} L).

11. NICS(0)zz values in 1o/1oH

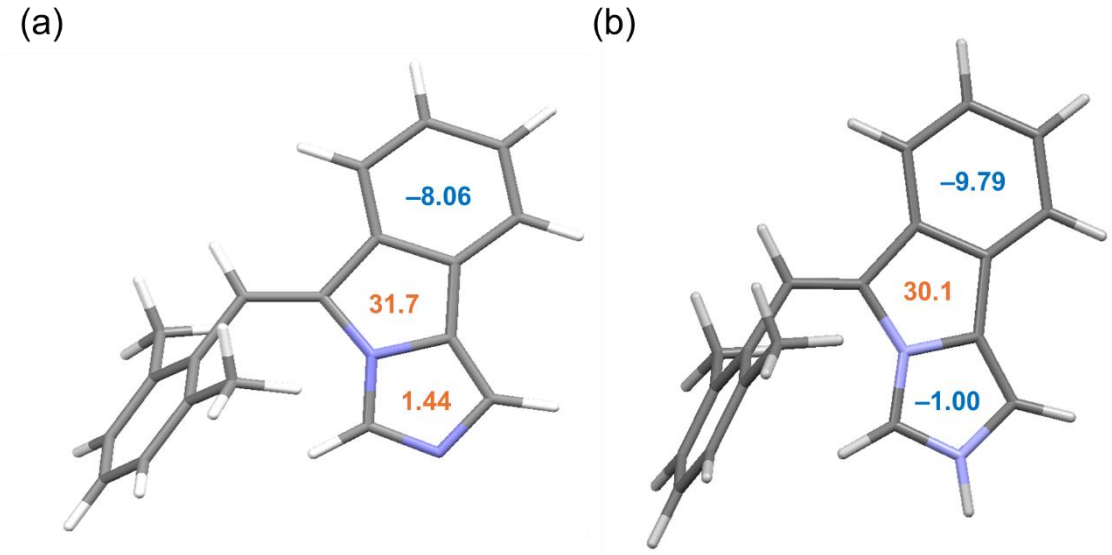

Figure 31. NICS(0)zz values in the optimized structures of (a) **1o** and (b) **1oH**. Negative NICS(0)zz values indicate aromaticity (blue colour), whereas positive values indicate antiaromaticity (orange colour).

12.Molecular orbitals

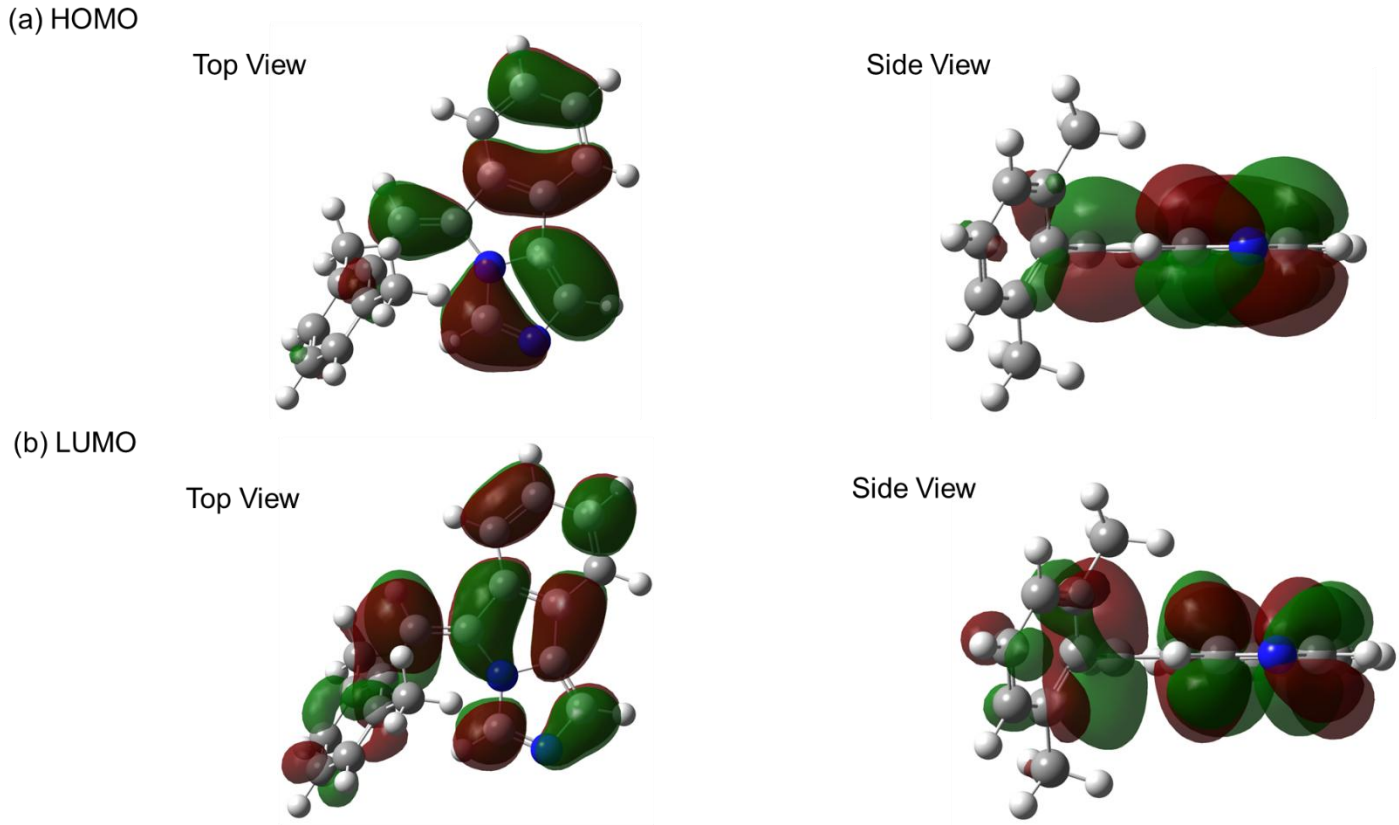

Figure 32. HOMO and LUMO of **1o**. Calculation level: M062x/6–311 + G(d,p).

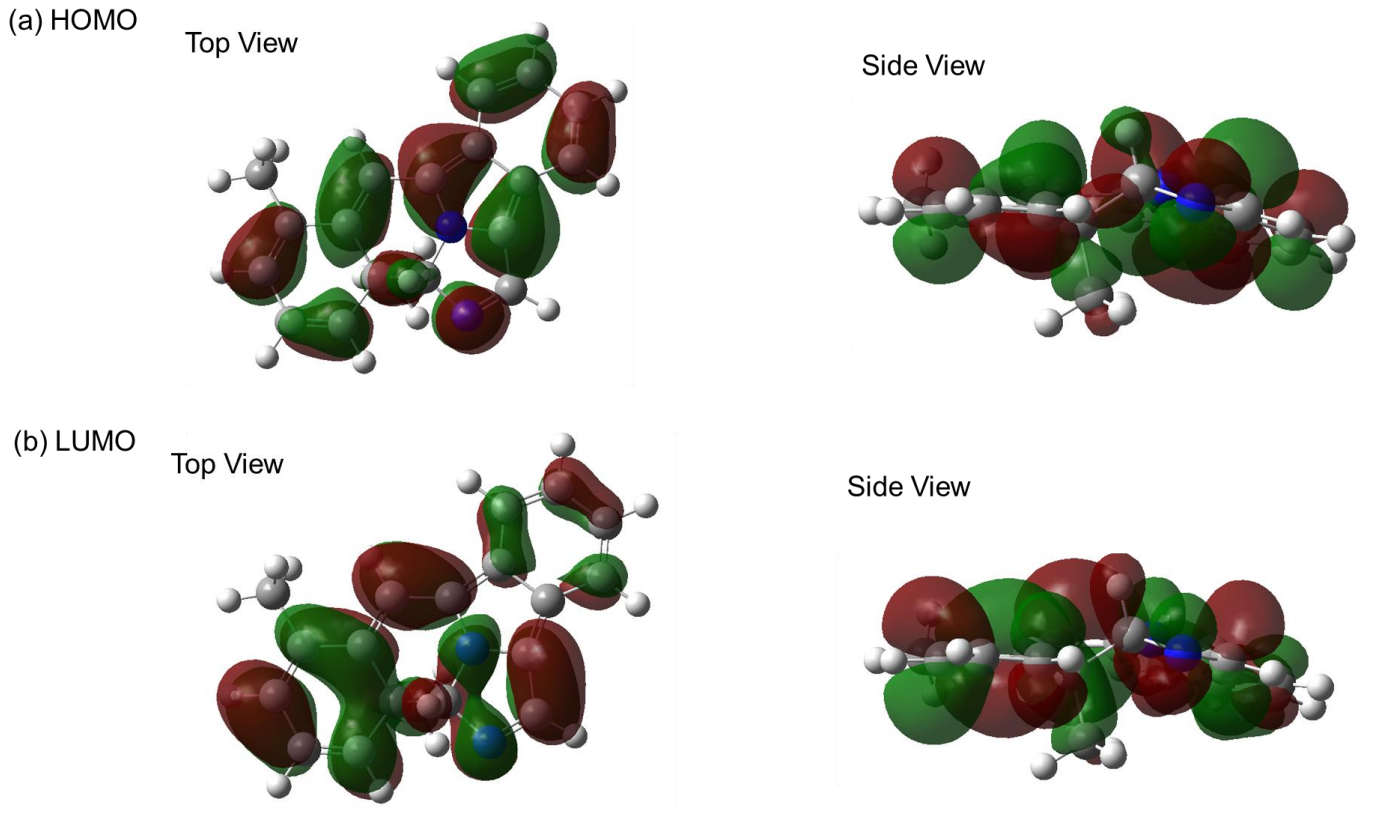

Figure 33. HOMO and LUMO of **1c**. Calculation level: M062x/6–311 + G(d,p).

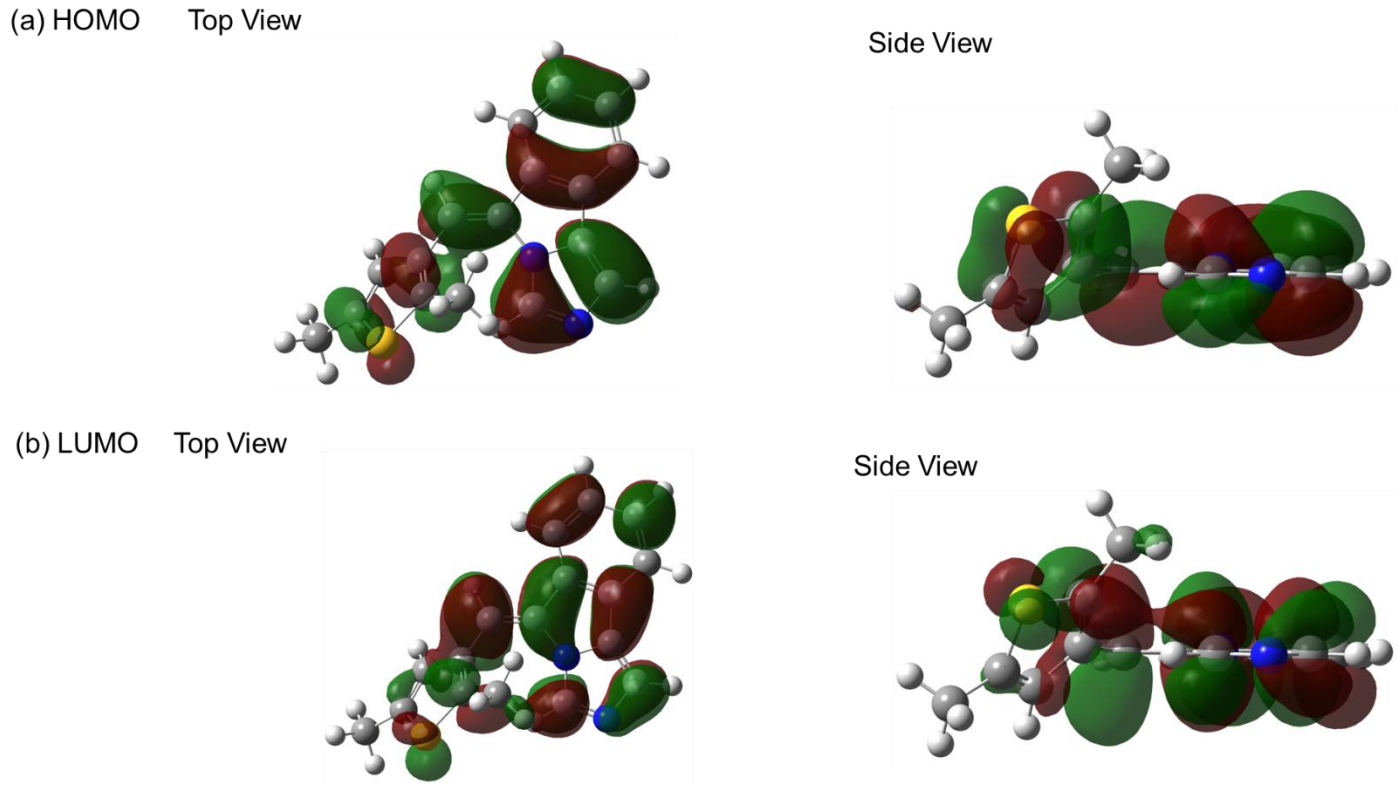

Figure S34. HOMO and LUMO of **2o**. Calculation level: M062x/6–311 + G(d,p).

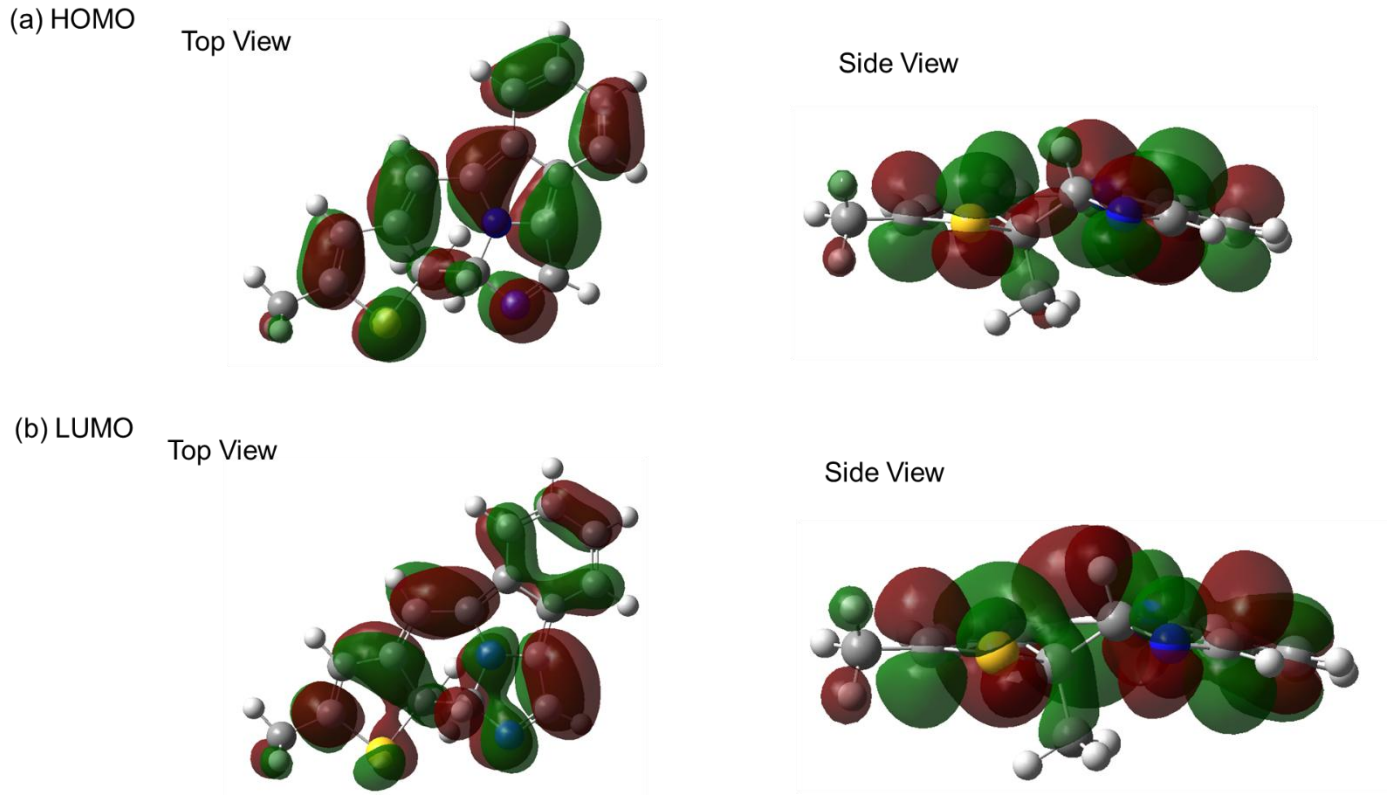

Figure S35. HOMO and LUMO of **2c**. Calculation level: M062x/6–311 + G(d,p).

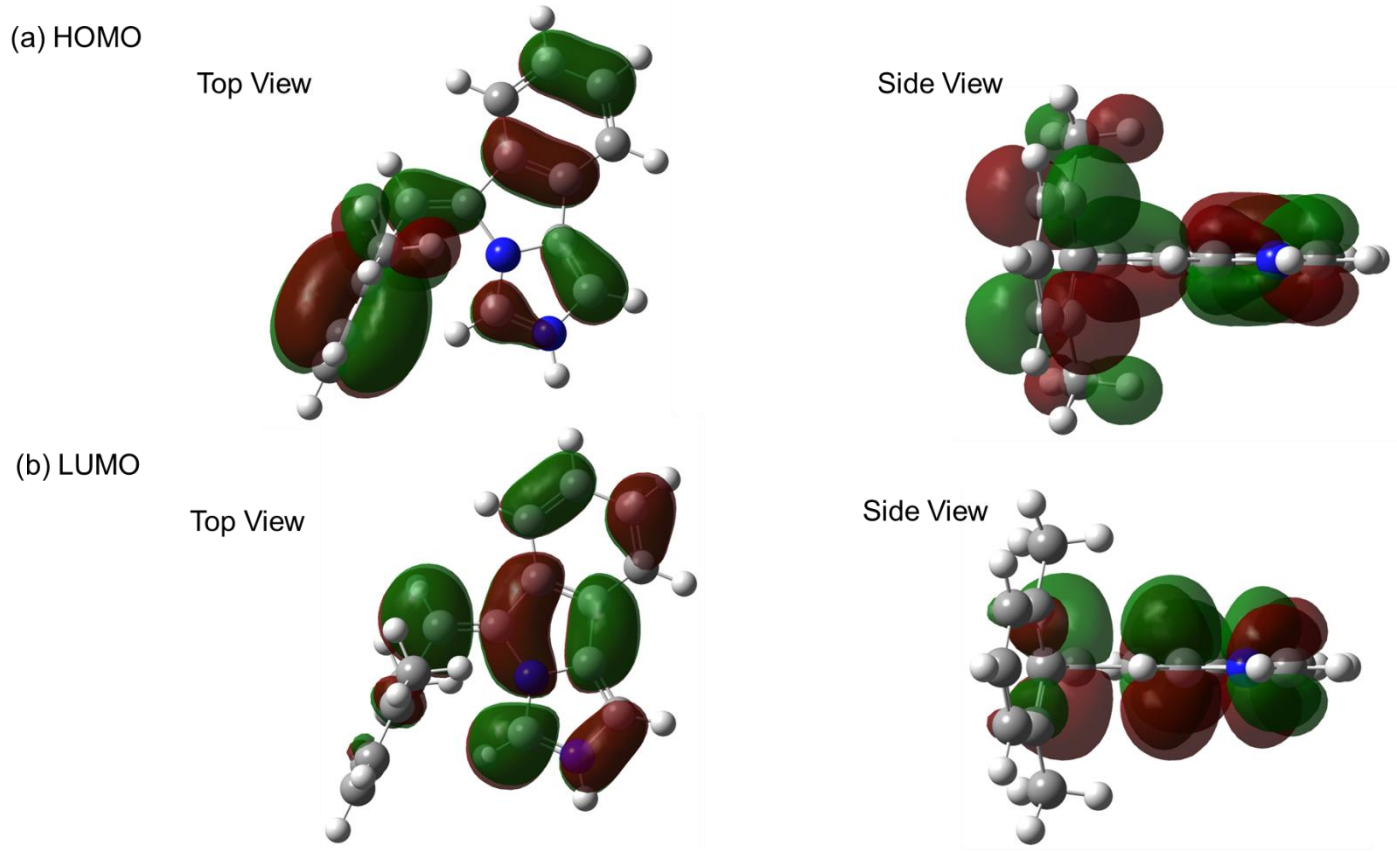

Figure S36. HOMO and LUMO of **1oH**. Calculation level: M062x/6–311 + G(d,p).

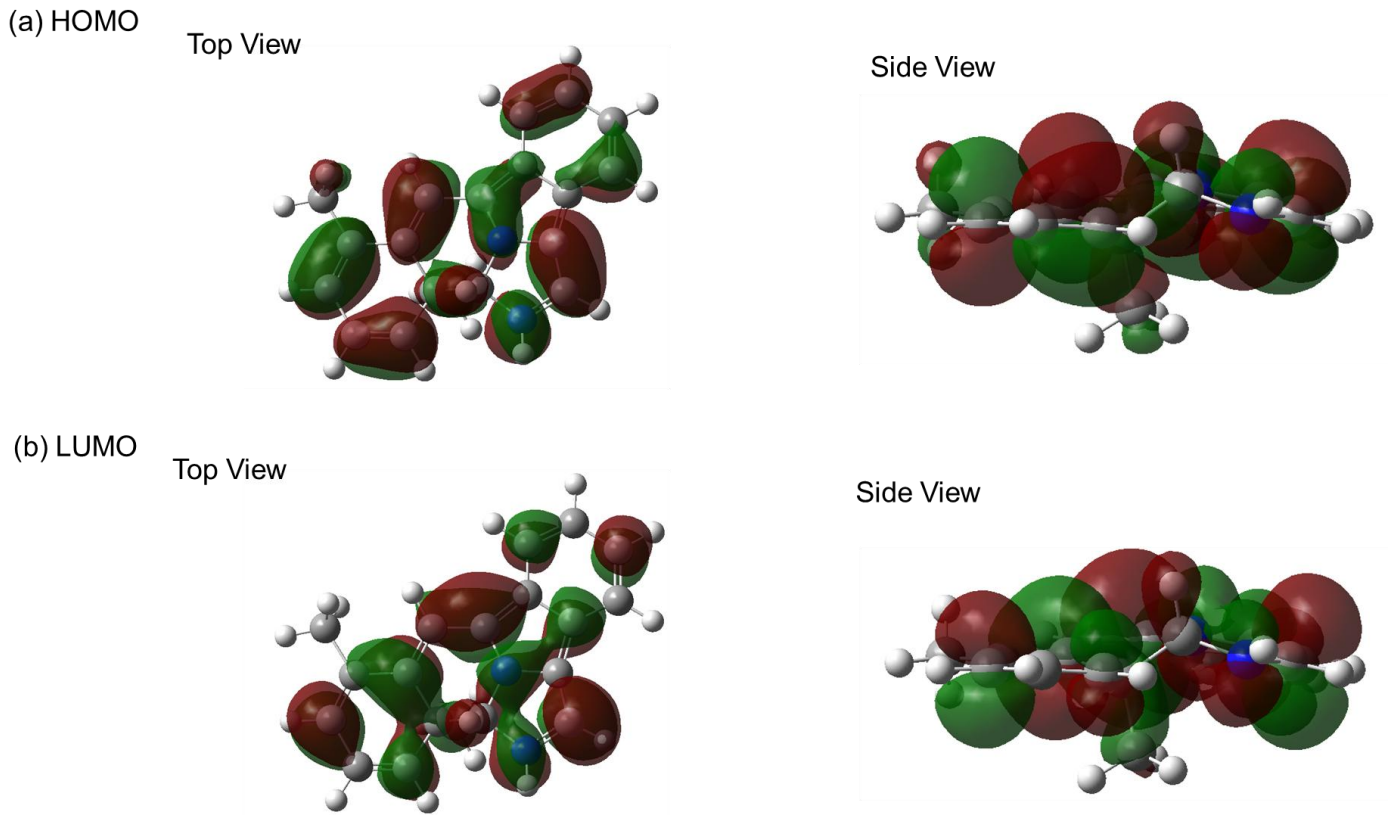

Figure S37. HOMO and LUMO of **1cH**. Calculation level: M062x/6–311 + G(d,p).

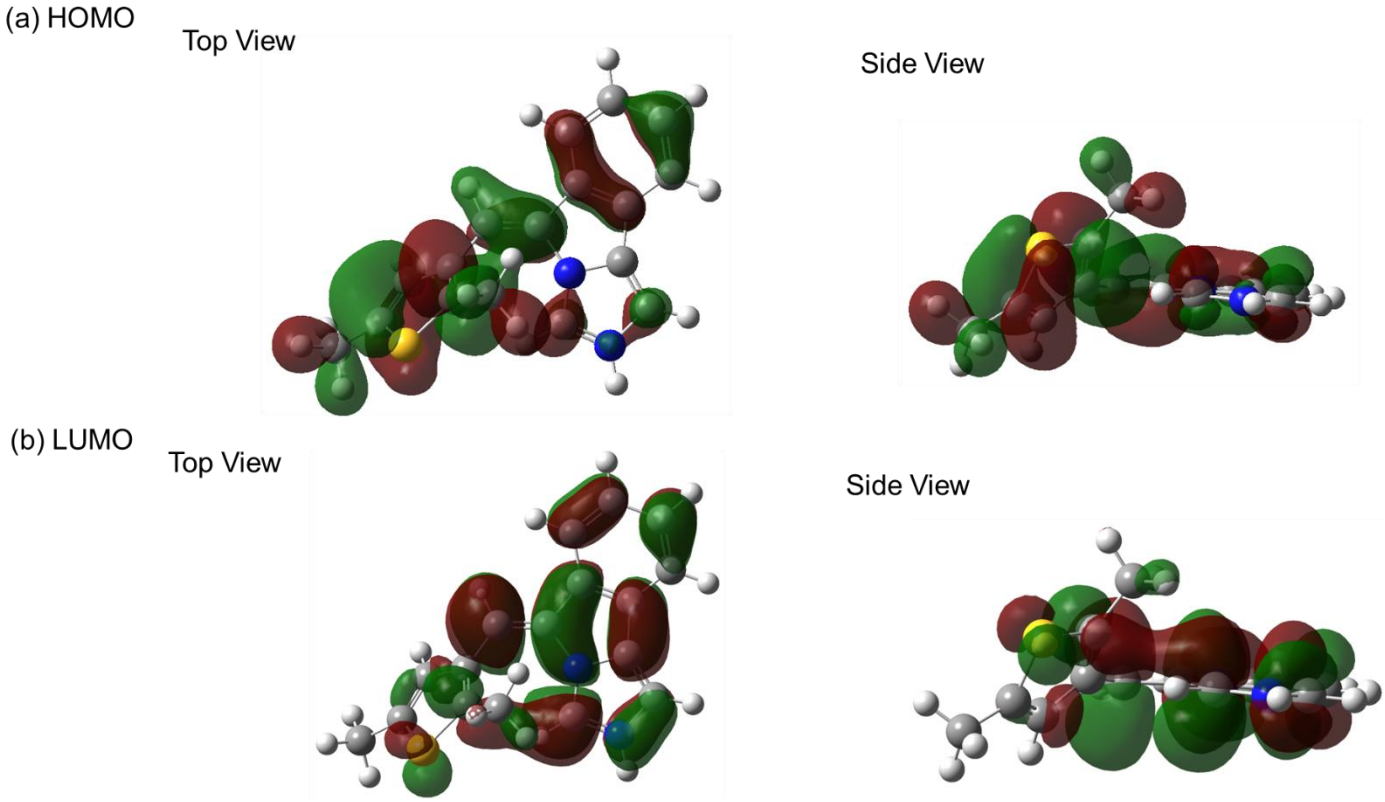

Figure S38. HOMO and LUMO of **2oH**. Calculation level: M062x/6–311 + G(d,p).

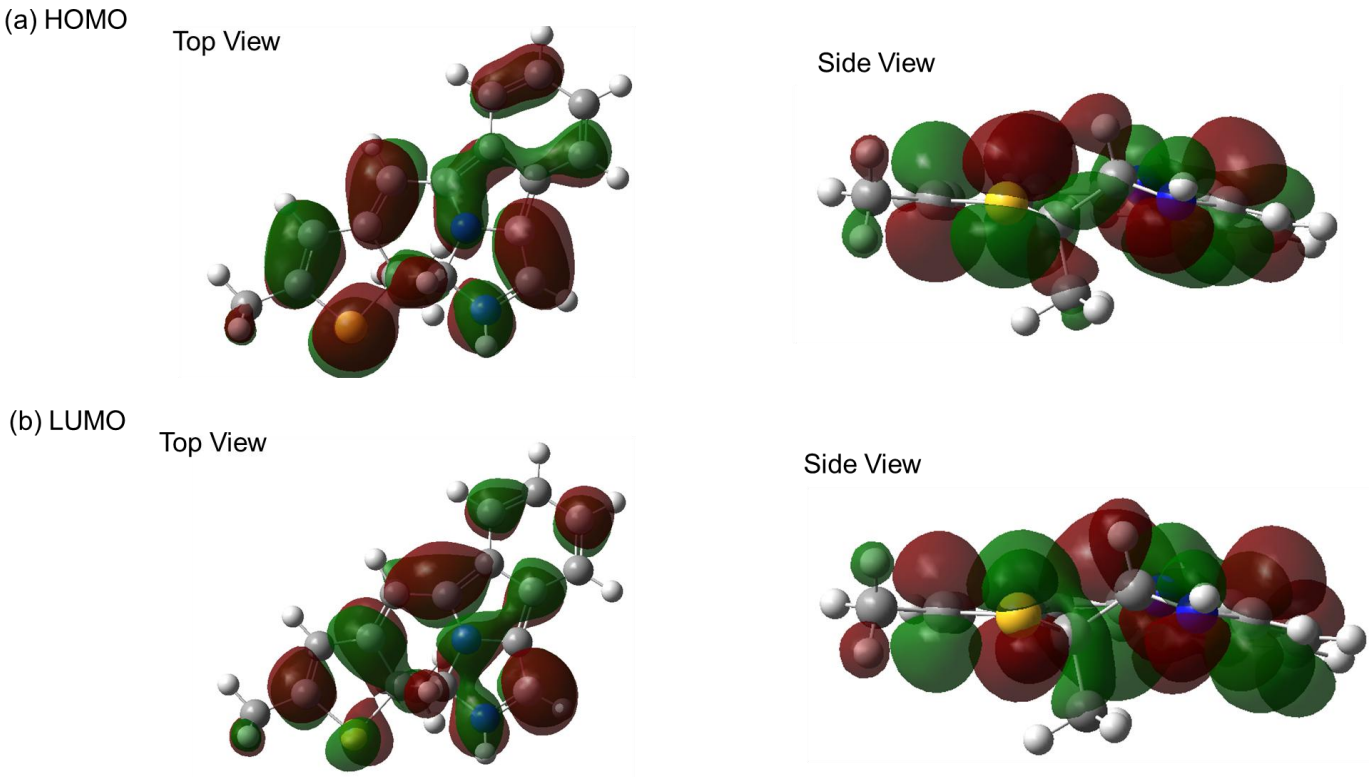

Figure S39. HOMO and LUMO of **2cH**. Calculation level: M062x/6–311 + G(d,p).

13. Potential energy surface

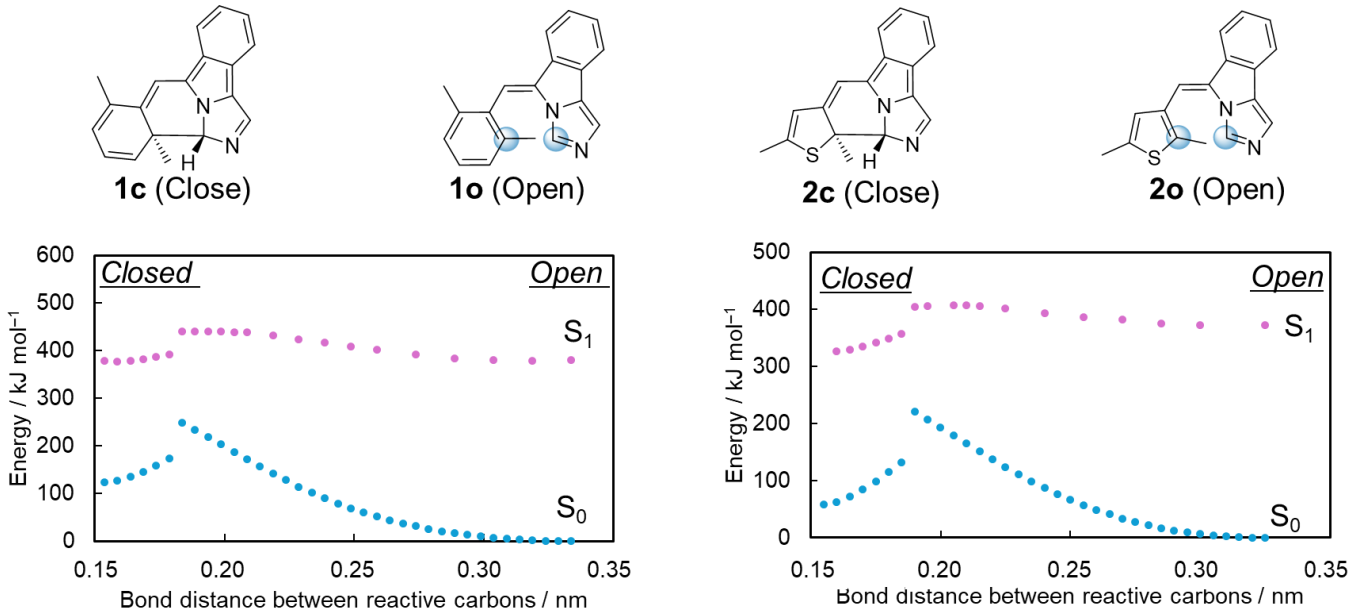

Figure S40. Potential energy surfaces (PES). The ground-state (S_0) PES was obtained at the UωB97X-D/6-311+G(d,p) level of theory, and the excited-state (S_1) PES was computed using TD-DFT at the ωB97X-D/6-311+G(d,p) level.

14. Changes in bond distances on the S_0 surface

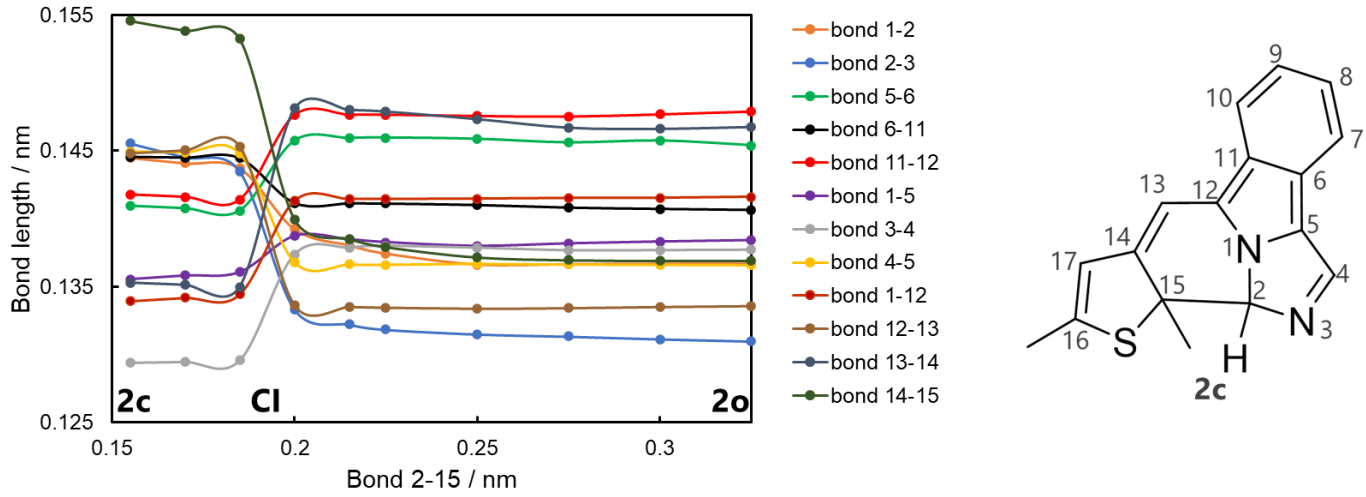

Figure S41. Changes in bond distances of **2o**/**2c** on the S_0 surface calculated by the scan method. Calculation level: UωB97XD/6-31+G(d,p).

15. IRC of 2cH/2oH

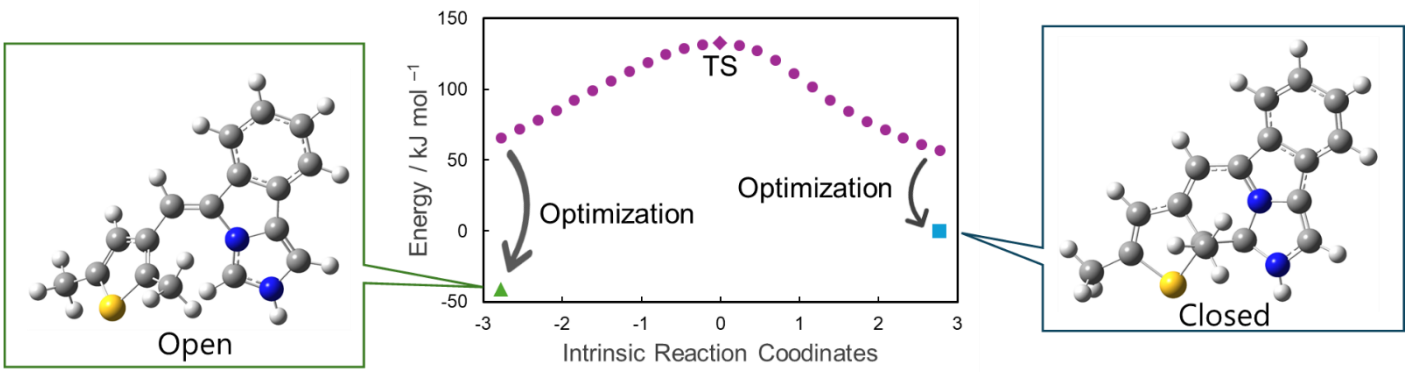

Figure S42. The intrinsic reaction coordinate (IRC) of **2cH**/**2oH** in ground state, i.e.,relaxing from transition state (TS). Relaxed from the initial TS to give the open- and closed-ring isomers (Open and Closed) in each direction.

16. Reference

S1) Taichi Muto, Mihoko Yamada, Shohei Katao, Fumio Asanoma, Didier Bourissou, Gwénaël Rapenne and Tsuyoshi Kawai, Chem. Eur. J. 2025, 31, e202501284.